Dual-porosity model of solute diffusion in biological tissue modified by electroporation

CrossMark

Samo Mahnič-Kalamiza [a,b,*], Damijan Miklavčič [b], Eugène Vorobiev [a]

[a] University of Technology of Compiègne, Centre de Recherches de Royallieu, BP 20529, 60205 Compiègne Cedex, France
[b] University of Ljubljana, Faculty of Electrical Engineering, Tržaška c. 25, SI-1000 Ljubljana, Slovenia

ARTICLE INFO

ABSTRACT

In many electroporation applications mass transport in biological tissue is of primary concern. This paper presents a theoretical advancement in the field and gives some examples of model use in electroporation applications. The study focuses on post-treatment solute diffusion.

We use a dual-porosity approach to describe solute diffusion in electroporated biological tissue. The cellular membrane presents a hindrance to solute transport into the extracellular space and is modeled as electroporation-dependent porosity, assigned to the intracellular space (the finite rate of mass transfer within an individual cell is not accounted for, for reasons that we elaborate on). The second porosity is that of the extracellular space, through which solute vacates a block of tissue.

The model can be used to study extraction out of or introduction of solutes into tissue, and we give three examples of application, a full account of model construction, validation with experiments, and a parametrical analysis. To facilitate easy implementation and experimentation by the reader, the complete derivation of the analytical solution for a simplified example is presented.

Validation is done by comparing model results to experimentally-obtained data; we modeled kinetics of sucrose extraction by diffusion from sugar beet tissue in laboratory-scale experiments. The parametrical analysis demonstrates the importance of selected physicochemical and geometrical properties of the system, illustrating possible outcomes of applying the model to different electroporation applications. The proposed model is a new platform that supports rapid extension by state-of-the-art models of electroporation phenomena, developed as latest achievements in the field of electroporation.

1. Introduction

As shown by experiments on lipid bilayers, cells in suspensions, monolayers and biological tissue, electric field can, if of sufficient strength, cause a significant increase in the conductivity and permeability of the lipid membrane [1]. This effect is known as electroporation and has been attributed to creation of aqueous pathways in the lipid bilayer [2,3]. Throughout this paper we will assume that solute diffusivity in biological tissue can be enhanced by electroporation by means of applying one or a series of electroporative pulses of a particular amplitude and duration to the tissue.

Electroporation is studied in a number of diverse fields [4,5], such as in biomedicine for gene delivery [6–8], electrochemotherapy [9–12], transdermal drug delivery [13–16], or tumor ablation by irreversible electroporation [17,18]; in food engineering and chemistry for increasing extraction yield [19–21], improving the quality of extract [22–24], or food preservation [25–27]; as well as in environmental sciences for waste water treatment [28,29], lipid extraction [30], or plant growth stimulation [31,32]. In all domains we encounter the need for introducing into or extracting out of the biological cells the solutes of interest. These range from small chemical compounds such as sucrose molecules [33,34] in food processing to larger and more complex drugs for electrochemotherapy [35] and to still larger lipids [30], and finally to the very large RNA and DNA molecules in gene therapy research [36]. This variability poses a challenge when determining parameters of electroporation, and recommended treatment protocols for their respective applications [37,38], as well as protocol optimization [39], are subjects of intensive research.

The problem of mass transfer during and after application of electroporative pulses has been treated both experimentally [40–42] and theoretically [43–48], and in studies combining both approaches [49–52], but mainly employing less complex systems, e.g. cell suspensions [43] and monolayers of cells [50,53]. This reservation to systems of lesser complexity seems to hold particularly true for theoretical models.

* Corresponding authors at: Université de Technologie de Compiègne (UTC), Département de Génie des Procédés Industriels, Laboratoire Transformations Intégrées de la Matière Renouvelable, Centre de Recherches de Royallieu, BP 20529, 60205 Compiègne Cedex, France. Tel.: +33 6 52 17 30 92.
E-mail addresses: samo.mahnic@utc.fr, samo.mahnic@fe.uni-lj.si, samo.mahnic@gmail.com (S. Mahnič-Kalamiza).

In many important electroporation applications, e.g. electroche-
motherapy or extraction of valuable compounds from plant tissue, the
object of interest is heterogeneous tissue composed of cells in close
contact that are of variable size [54], shape [55], and that may be inter-
connected via intercellular junctions [56]. These factors influence – to a
varying extent – the electroporation process, electrotransfer and diffu-
sion of solute, both during and after electroporation. Additionally,
membrane contacts of adjacent cells in animal tissues reduce the effects
of the electric field, as shown by studies on dense cell suspensions [57],
while the effects of the cell wall in plant tissues and the porosity of
extracellular space have not yet been evaluated in relation to electropo-
ration. Furthermore, we often come across clearly defined sources and/
or sinks of observed solute. These introduce the need for not only
temporal observation and inclusion of reaction kinetics in the model
[45], but also the need to determine the spatial distribution of solute
concentration in tissue [46].

With respect to electroporation and its effects on cell membrane
transport, we have to examine the nature of solute transported in rela-
tion to the electric pulse parameters and electrical properties of tissue
[58,59], as well as the local electric field distribution [60,61]. Several
mechanisms of transport were reported in addition to free diffusion,
such as electrokinetic effects facilitated by the electric field. The list of
these comprises electrophoresis [45], electroosmosis [47] and FASS
(Field-Amplified Sample Stacking) [45,62], as well as cellular and
membrane processes such as endocytosis [63]. The importance of indi-
vidual mechanisms depends not only on the nature of solute, but also
on the parameters of delivered electric pulses [48,64] and the time of
observation of the system. The time of observation is important since
it delineates two modeling paradigms — we either model periods dur-
ing as well as after electric pulse application with electrokinetic effects,
or we focus on the post-pulse period only, where the dominant mass
transport is by diffusion through long-lived pores [50,59,65].

The model that we present in this paper is an attempt at advancing
the basis of the theoretical modeling of mass transport in electropora-
tion applications. Tissue is modeled as a dual-porosity medium. One
medium is represented by the intracellular and the other by extracellu-
lar space, with cell membrane separating the two media. It has been
developed in order to model experimental results in a particular case
of plant tissue electroporation with purpose of solute extraction, but
can, with modification, also be applied to applications in biomedicine
(e.g. electrochemotherapy) and other fields of electroporation research
where there is a need to model solute transport on the level of tissue.
In this first attempt at building a dual-porosity model, we are
concerned only with free diffusion of small molecules (several kDa)
post-pulse, when the effects of the electric field are either no longer
present or are negligible. We have, however, coupled diffusion with
the effects of electroporation through its effects on membrane
permeability.

In our model study, the transport modeled will be that of sucrose ex-
tracted from sugar beet tissue. We are including a comparison of model
results with experimental data as model validation and an illustration of
the model application, while also presenting a parametric study. By
means of the latter we attempt to both analyze the influence of some
of the electroporation parameters on model predictions as well as
gauge the sensitivity of the model to potential errors in parameter
estimation.

Since the model presented is a proof of concept and the interpreta-
tion of its results has illustrative value, we have kept the model in
this first account simple enough, so that an analytical solution could
be readily found and discussed. A clear and complete demonstration
of applying the model to problems in a different field of electropora-
tion research, e.g. in electrochemotherapy or intra/transdermal drug
transport, requires and deserves a study and paper of its own. For
brevity, we therefore only present, in theory, the necessary modifica-
tions to the model, which we believe are necessary to adapt it to
problems of drug diffusion in tissues for biomedical applications.

For a schematic representation on how the paper explores the
dual-porosity modeling paradigm and how its contents are divided
into subsections, see Fig. 1.

2. Theoretical formulation of the problem, model construction, and its application

2.1. System of solute diffusion equations in a dual-porosity medium

The rationale behind the use of the following model equations
comes from the theory of porous media [66], more precisely from the
observations of liquid flow in soils and fractured rocks. From the
mathematical point of view, we exploit the analogy of fluid flow and
heat transfer in porous media with problems in mass transport by
diffusion [67]. The same (mathematical) treatment is thus applicable
that has been thoroughly studied in problems of heat and mass transfer
in porous media [68,69].

We model a block of tissue as composed of essentially two media,
the extracellular and the intracellular. At their respective volume
fractions, they occupy the same block of tissue, as is illustrated by
Fig. 2. Tissue is modeled as comprising cells' interior volume that collec-
tively forms the intracellular space. The intracellular space is separated
by the cell membrane from the extracellular space, which comprises
primarily the cell wall (in plants) or collagen (e.g. in skin tissue), as
well as miscellaneous and other biomolecules in addition to the
entrapped liquid (and air in plants) in the intercellular compartments.
Electric field primarily acts on membranes, rendering them permeable
thus effectively affecting the porosity of the intracellular space; electro-
poration of membranes is therefore enabling diffusive transport of
solutes through the membrane.

If we imagine a sample of tissue of finite thickness (e.g. a few
hundred layers of cells), we can identify two diffusive flows of solute.
Assuming that initially there is a higher concentration of solute within
the cells as compared to the extracellular space, first, the solute has to
diffuse out of individual cells (i.e. from intracellular space) into the
extracellular space. This is the transmembrane flow. Second, the solute
diffuses through the block of tissue via the extracellular route; this
diffusion is driven by the gradient that appears in the block of tissue
due to conditions at the tissue sample boundaries. In extraction applica-
tions, the boundary condition can ideally be assumed constant and
equal to zero (i.e. infinite dilution into surrounding solvent). In
electrochemotherapy or transdermal drug transfer applications, the
boundary condition is non-zero, i.e. constant or time-varying (depending
on application), e.g. a skin reservoir of finite capacity; or a local drug
plasma concentration dependent on locally (un)obstructed blood flow,
etc. The extracellular path results in an extracellular flow in the presence
of concentration gradients imposed by the boundary and initial
conditions. Solute leaving the cells results in a decrease of intracellular
concentration, and an increase in extracellular concentration. On the
other hand, solute leaving the tissue sample in effect decreases extracel-
lular concentration. This gives us, for intrinsic concentration (i.e. concen-
tration averaged over the volume fraction of each phase) in extracellular
space and intracellular space respectively, the following set of partial
differential equations (PDEs):

$$\frac{\partial c_e(z,t)}{\partial t} - D_{s,e}\frac{\partial^2 c_e(z,t)}{\partial z^2} - \frac{1-\varepsilon}{\varepsilon}k\cdot[c_i(z,t)-c_e(z,t)] = 0 \qquad (1)$$

$$\frac{\partial c_i(z,t)}{\partial t} + k\cdot[c_i(z,t)-c_e(z,t)] = 0. \qquad (2)$$

In Eqs. (1)–(2), c_i and c_e denote intrinsic volume-averaged intracel-
lular and extracellular (respectively) molar concentrations in units
mol·m^{-3}, $D_{s,e}$ is the diffusion coefficient of solute species s in extracel-
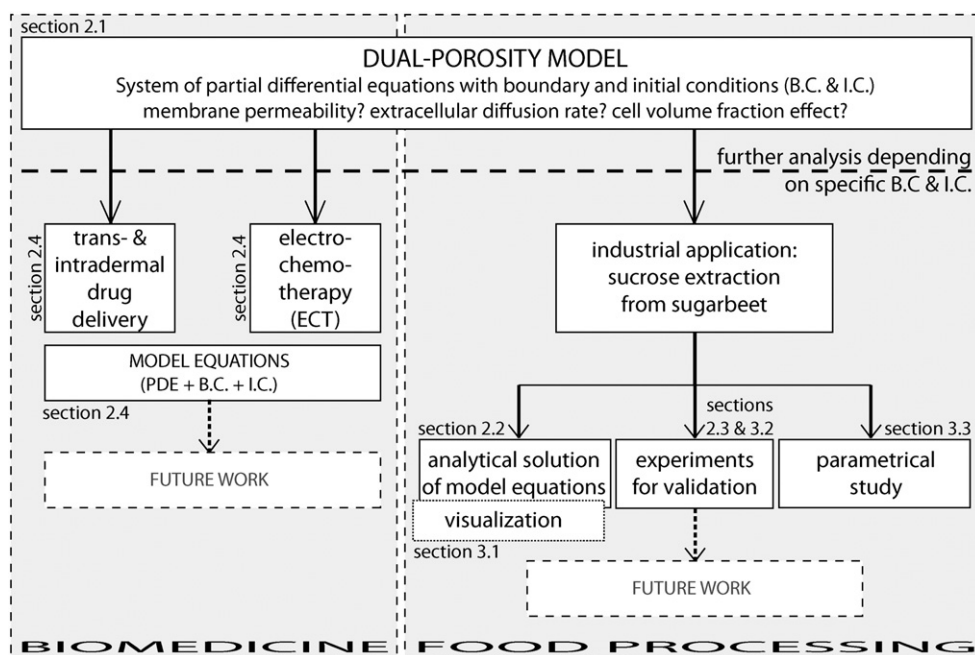lular space with units m^2·s^{-1}, z is the spatial coordinate aligned with

Fig. 1. The dual-porosity modeling paradigm as explored in this article.

(i.e. parallel to) the principal axis of diffusion, and $k(c_i - c_e)$ is the volume-averaged flow in units $mol \cdot m^{-3} \cdot s^{-1}$. This member as well as the multiplicative factor $(1 - \varepsilon)/\varepsilon$ will be further deconstructed and explained during the course of the following analysis. We have supposed only one principal axis of diffusion is relevant, and that is the axis perpendicular to the largest surface of the tissue sample. In other words, we have simplified the problem to one spatial dimension, our rationale supported by an assumption that the thickness of the studied block of tissue is small as compared to its largest surface. The model as given by Eqs. (1)–(2) does not account for convective flow or chemical reactions, but can readily be expanded with additional terms if necessary. The model geometry (as illustrated by Fig. 3) appears in a number of electroporation applications; in industrial extraction of solutes from plant tissues, tissue is sliced or grated into thin blocks or cossettes to facilitate faster diffusion; in transdermal drug delivery, skin patches can be modeled as thin reservoirs with large surface area in contact with the skin; while in subcutaneous tumor electrochemotherapy for example, large tumors not protruding deep into the subcutaneous tissue exhibit properties that can be, by in no means excessive stretch of imagination, approximated using the proposed model geometry.

The given system of model equations describes what is commonly referred to in the relevant established literature as a LNE (Local Non-Equilibrium) model. See e.g. [67] for a recent review of LNE models as applied in theory of mass transport in biological tissue modeled as a porous medium.

In order to support further theoretical treatment and procurement of an analytical solution, we must establish the following set of assumptions and simplifications: (i) — as indicated by Eq. (1), diffusion coefficient of solute in extracellular space is assumed to be constant. For spatial dependence, the second member in Eq. (1) has to be revised to $\partial/\partial z[D_{s,e} \cdot \partial c_e(z,t)/\partial z]$, rendering the system complex and cumbersome for analytical treatment, while for temporal dependence $D_{s,e} = f(t)$, a new timescale T has to be introduced, so that $dT = f(t) \, dt$. Fortunately, there are no strong arguments from the physics of the process point of view that would necessitate taking either spatial or temporal dependence of $D_{s,e}$ into account; (ii) — the tissue is modeled as consisting of perfectly spherical cells of radius R, collectively occupying a volume fraction F of the tissue block and forming the intracellular space. The rest of the volume is extracellular space, occupying the volume fraction $1 - F$. Thus, the porosity (ratio of void volume to total volume) denoted
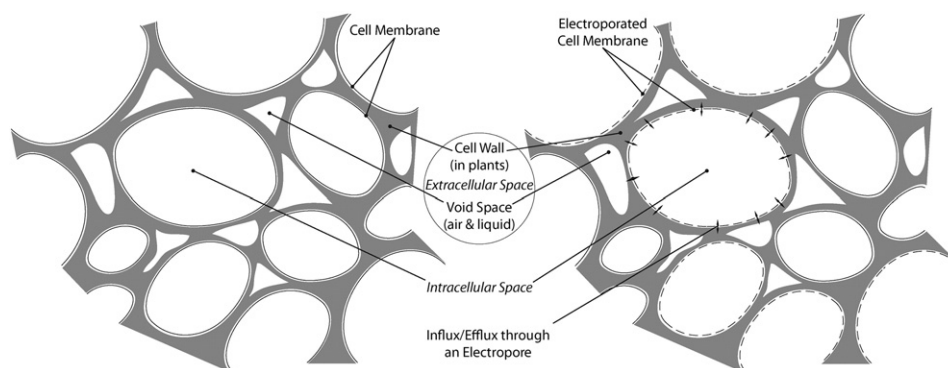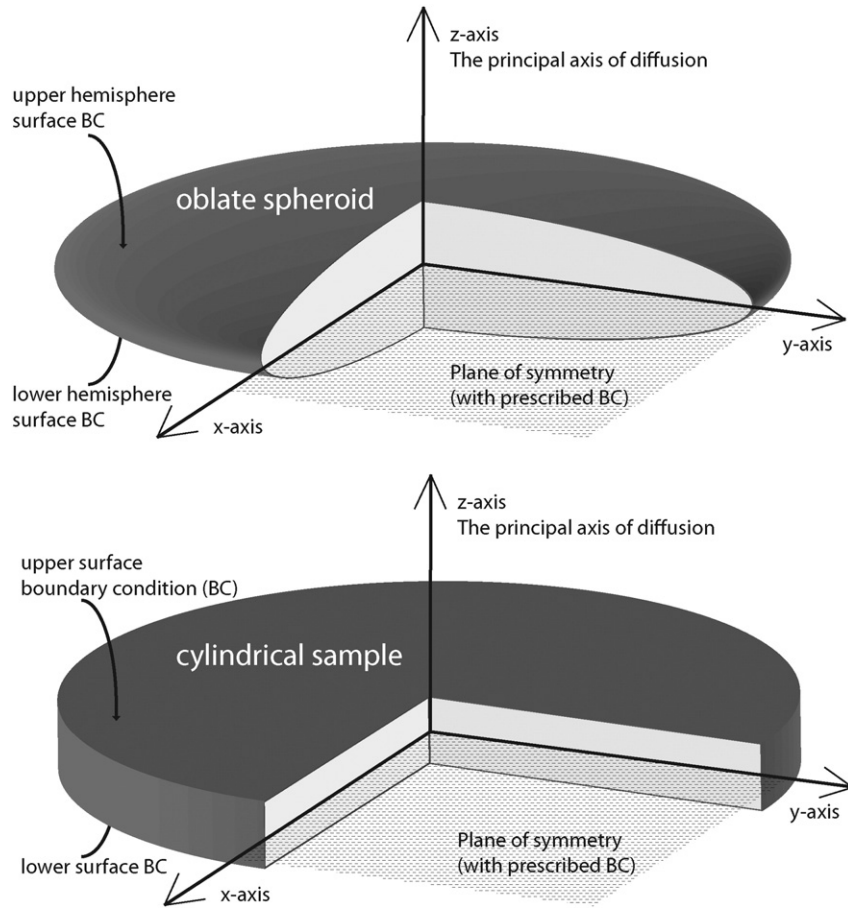

Fig. 2. Schematic representation of biological tissue, before electroporation (left) and after electroporation (right). Note that a segment (e.g. block) of modeled tissue may consist of several hundred layers of cells.

Fig. 3. Tissue sample geometry. An oblate spheroid modeling the subcutaneous tumor geometry; and a thin cylinder as a model of a sugar beet tissue sample as used in many laboratory experiments. The boundary conditions are prescribed either on the both surfaces or on one surface and at the central plane due to symmetry, depending on the modeled system.

ε is equal to $1 - F$; (iii) — the electrical field applied to the tissue during electroporation is assumed spatially homogeneous. This is a valid assumption for the bulk volume of tissue in an electroporation setup with parallel plate electrodes, or even a small block of tissue with an otherwise heterogeneous field distribution (local homogeneity); (iv) — since all cells are modeled as being of equal size and shape and the electrical field homogeneous throughout the modeled block of tissue, application of electroporating pulses to the tissue inflicts an equal distribution of pores, irrespective of the location of an individual cell in tissue; (v) — pores created by electroporation are of various sizes according to some statistical distribution. All further analysis operates with an *average size* of a pore created in the cellular membrane. The same logic of averaging applies to the *number of pores* created, which is assumed to be dependent only on electroporative pulse parameters (e.g. maximum field strength, number and duration of pulses, etc.) and not on local inhomogeneity (in either field strength, geometry or conductivity — these are considered homogeneous throughout the sample).

Returning now to the initial model Equations (1)–(2), we need to establish how volume-averaged intra-to-extracellular (i.e. transmembrane/pore) flow, denoted $k(c_i - c_e)$, depends on electroporation. We start by writing Fick's first law of diffusion for flow through pores in membrane of total (pore) area A_p in spherical geometry of an idealized spherical cell of radius R

$$j_{s,p} = -D_{s,eff} A_p \frac{dc}{dr}. \tag{3}$$

Integrating across the membrane where the gradient of concentration is non-zero, we obtain

$$j_{s,p} \int_R^{R+d_m} dr = -D_{s,eff} A_p \int_{c_i}^{c_e} dc$$

giving

$$j_{s,p} = \frac{D_{s,eff} A_p}{d_m} (c_i - c_e) \tag{4}$$

where d_m is membrane thickness on the order of several nanometers, and $D_{s,eff}$ is the effective diffusion coefficient of solute species s through a single pore in the cell membrane, which can be approximated as

$$D_{s,eff} = D_{s,0} y_s \tag{5}$$

where $D_{s,0}$ is the diffusion coefficient of solute species s in water at a given temperature and y_s is the dynamic hindrance coefficient, accounting for hydrodynamic drag and steric exclusion effects.

The change in concentration of solute in intracellular space is entirely due to the trans-pore flow of solute into the extracellular space, i.e.

$$\frac{\partial c_i}{\partial t} = \frac{j_{s,p}}{V_i}. \tag{6}$$

If the pore flow $j_{s,p}$ is that across a single cell membrane, volume V_i is that of one cell and equals $V_i = 4\pi R^3/3$. Since the surface of a single cell A_0 is $4\pi R^2$, we can rewrite Eq. (6) as

$$\frac{\partial c_i}{\partial t} = \frac{3j_{s,p}}{A_0 R} = \frac{3D_{s,eff}f_p}{d_m R}(c_i - c_e) \tag{7}$$

where f_p is the pore surface fraction ratio calculated as A_p/A_0. This formulation using pore surface fraction ratio is useful, as this construct is often encountered in relevant literature (see e.g. [65]). Note that the pore area A_p is the total pore area per cell, and can be expressed as $A_p = \pi N_p r_p^2$, where N_p is the number of pores per cell and r_p the average radius of a single pore.

Comparing now Eq. (2) with Eq. (7), flow coefficient k (also termed mass transfer coefficient) can immediately be expressed as

$$k = \frac{3D_{s,eff}f_p}{d_m R} = P\frac{3}{R} \tag{8}$$

where P is the membrane permeability coefficient [70] and the term $3/R$ accounts for spatial averaging of transmembrane flow within the volume of a single cell and its exact value results from the idealized spherical geometry.

Furthermore, if the volume fraction F of cells in tissue would be exactly 0.5, the transmembrane flow would result in a change in intrinsic intracellular concentration equal to the change in intrinsic extracellular concentration. However, since in tissue in general the cells can occupy a significantly larger (e.g. in plant tissues [71]) or smaller (in e.g. tumor tissues [72]) volume fraction, as compared to extracellular space, the flow of solute out of the cells will also cause a significantly larger or smaller (but proportional) change in intrinsic extracellular concentration, as compared to the change in intrinsic intracellular concentration. Neglecting for a moment extracellular diffusion (in Eq. (1)), we write an equation analogous to Eq. (6), but for the extracellular space

$$\frac{\partial c_e}{\partial t} = \frac{j_{s,p}}{V_e} = \frac{j_{s,p}V_i}{V_e V} = \frac{V_i}{V_e}k \cdot (c_i - c_e) = \frac{1-\varepsilon}{\varepsilon}k \cdot (c_i - c_e) \tag{9}$$

where we have taken into account that in homogeneous tissue, for any arbitrarily chosen, finite and limited (i.e. on the order of comprising only several cells) volume of tissue ΔV, intracellular volume V_i to total volume ΔV ratio can be expressed as $F = 1 - \varepsilon$, and extracellular V_e to ΔV ratio as $1 - F = \varepsilon$. Note that if flow coefficient k were defined using extracellular volume as opposed to the intracellular, the factor

$(1 - \varepsilon)/\varepsilon$ would not be present in Eq. (1). Instead, k would have been multiplied by $\varepsilon/(1 - \varepsilon)$ in Eq. (2), giving exactly the same model results.

What remains is to explain the behavior of the dynamic hindrance coefficient y_s. This coefficient captures the effects that hinder solute diffusion through an aqueous pore due to comparable size of the solute molecule to that of the pore as well as any effects of electrical forces due to net surface charges on pore walls and the solute. A number of models have been proposed to describe hindered diffusion through aqueous pores, and comprehensive reviews were published by Deen [73] and Dechadilok and Deen [74]. The suitability of a particular model depends on the application, due to the varying physicochemical properties of the solute of interest that are of primary importance. For the model study with sucrose that we present later on in this paper, we follow a recent study by Liesche and Shulz [75], who modeled sucrose diffusion through plasmodesmata and used a model already proposed in [74], which is based on a modified model previously described by Higdon and Muldowney [76]. According to this model, if λ_r is the solute to pore ratio, $\lambda_r = r_s/r_p$, the hindrance coefficient y_s as a function of λ_r can be given as

$$y_s(\lambda_r) = 1 + \frac{9}{8}\lambda_r \ln\lambda_r - 1.56034\lambda_r + 0.528155\lambda_r^2 + 1.91521\lambda_r^3$$
$$- 2.81903\lambda_r^4 + 0.270788\lambda_r^5 + 1.10115\lambda_r^6 - 0.435933\lambda_r^7. \tag{10}$$

A slightly simpler but comparable alternative is the Renkin equation [77], given by

$$y_s(\lambda_r) = 1 - 4.1\lambda_r + 5.2\lambda_r^2 - 0.01\lambda_r^3 - 4.18\lambda_r^4 + 1.14\lambda_r^5$$
$$+ 1.9\lambda_r^6 - 0.95\lambda_r^7. \tag{11}$$

Both functions, plotted for λ_r within the interval [0, 1] and within [0.5, 0.9], are presented in Fig. 4. As evident, the difference in model results for $\lambda_r \geq 0.3$ is practically insignificant.

In order to determine $D_{s,e}$, the solute diffusion coefficient in extracellular space, in general we would have to consider the tortuosity of the extracellular pathways as well as the porosity. However, since we are operating with intrinsic concentrations c_i and c_e, and not concentrations averaged to the total tissue volume (see [67], Section 3.2.1.1 for a detailed explanation of the difference), $D_{s,e}$ is not a function of porosity. It is, however, reduced considerably and to a non-negligible extent due to the tortuosity of the extracellular pathways. In our simplified model of spherical cells, the solute has to diffuse, in order to move a net distance dz along z in the extracellular space, around the model spherical cell. On the level of a single cell, to diffuse by one cell diameter
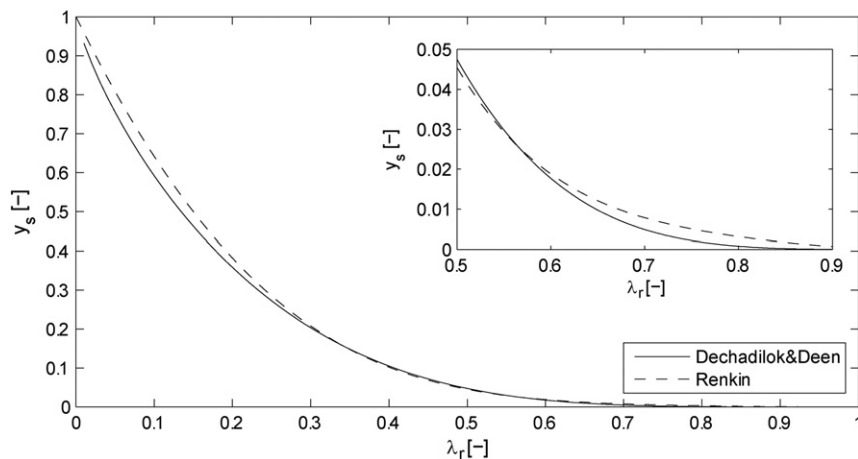

Fig. 4. Effect of steric exclusion and hydrodynamic drag on the dynamic hindrance coefficient y_s of solute through a pore in the membrane-model comparison. The insert is a closer look for λ_r within the bounds [0.5, 0.9].

$2R$ along z, it has to cover a total distance of πR along the hemi-sphere. The tortuosity τ then equals $\tau = \pi R/2R = \pi/2$. The extracellular diffusion coefficient, if intrinsic concentrations are observed, is then $D_{s,e} = D_{s,0}/\tau = D_{s,0} \cdot 2/\pi$, where $D_{s,0}$ is the diffusion coefficient of solute species s in water at a given temperature.

2.2. Analytical solution

In some, albeit few, electroporation applications we are operating with a more or less homogeneous tissue that can also be relatively homogeneously treated with electroporation due to the particular implementation of the treatment application. Such is the case in some industrial applications of electroporation (e.g. extraction, drying, impregnation). This makes coefficients $D_{s,e}$ and k constant in space and time-invariant. Under such conditions, an analytical solution of the dual-porosity model can be obtained. The complete derivation is given in Appendix A.

In order to solve the system of Eqs. (1)–(2), we need to define initial and boundary conditions. To demonstrate the use of the dual-porosity model and provide validation, we will study sucrose extraction from vegetable (sugar beet) tissue. For the purposes of this study, we will model a thin slice of tissue pretreated with electroporation and suspended into a diffusion chamber in a prescribed solid-to-liquid volume ratio, and the liquid medium well stirred. Such setups can readily be found described in the literature, e.g. in [20–22]. The geometrical data for the tissue samples can be found in the table of parameters, Table 1.

We assume that sucrose is initially homogeneously distributed within the intracellular phase and within the extracellular phase (but not necessarily equal in the two media), giving initial conditions

$$c_e(z, 0) = c_{e0} \tag{12}$$

$$c_i(z, 0) = c_{i0}. \tag{13}$$

During the modeled diffusion experiment, a tissue sample is submerged in distilled water which is constantly agitated. The setup allows us to model one half of a tissue sample due to symmetry. We have the following boundary conditions (BC) for extracellular concentration (l is the thickness of the tissue sample)

$$\left. \frac{\partial c_e(t)}{\partial z} \right|_{z=0} = 0 \tag{14}$$

$$c_e(t)|_{z=l/2} = 0. \tag{15}$$

The BC for intracellular concentration at the plane of symmetry (mid-section of tissue block at $z = 0$) also equals 0 (no-flux boundary)

$$\left. \frac{\partial c_i(t)}{\partial z} \right|_{z=0} = 0 \tag{16}$$

while the BC for intracellular concentration at the sample surface is not immediately apparent. It is governed by Eq. (2), and can easily be determined due to the homogeneous BC just given by Eq. (15). Writing Eq. (2) for $z = l/2$, we get an ordinary differential equation

$$\left[\frac{dc_i(t)}{dt} \right]_{z=l/2} + k[c_i(t)]_{z=l/2} = [c_e(t)]_{z=l/2} = 0 \tag{17}$$

with initial condition as already given by Eq. (13). The solution of this ordinary differential equation, as can easily be verified, is

$$c_i(t)|_{z=l/2} = c_{i0}e^{-kt}. \tag{18}$$

The system of Eqs. (1)–(2) with initial and boundary conditions as defined above represents a mathematical model of solute diffusion according to the theory of mass transfer in porous media.

The solution of the PDE system is

$$c_e(z,t) = \frac{4c_{i0}}{\pi} \sum_{n=0}^{\infty} \frac{(-1)^n}{2n+1} \cos(\lambda_n z) \left(C_{n,1} e^{\gamma_{n,1} t} \left(\frac{\gamma_{n,1}}{k} + 1 \right) + C_{n,2} e^{\gamma_{n,2} t} \left(\frac{\gamma_{n,2}}{k} + 1 \right) \right) \tag{19}$$

$$c_i(z,t) = \frac{4c_{i0}}{\pi} \sum_{n=0}^{\infty} \frac{(-1)^n}{2n+1} \cos(\lambda_n z) \left(C_{n,1} e^{\gamma_{n,1} t} + C_{n,2} e^{\gamma_{n,2} t} - e^{-kt} \right) + c_{i0} e^{-kt} \tag{20}$$

where

$$C_{n,1} = \frac{\left(\frac{c_{e0}}{c_{i0}} - 1 \right) k - \gamma_{n,2}}{\gamma_{n,1} - \gamma_{n,2}} \tag{21}$$

$$C_{n,2} = \frac{\left(1 - \frac{c_{e0}}{c_{i0}} \right) k + \gamma_{n,1}}{\gamma_{n,1} - \gamma_{n,2}} \tag{22}$$

and

$$\gamma_{n_{1,2}} = \frac{-\left((\delta+1)k + \lambda_n^2 D_{s,e} \right) \pm \sqrt{\left((\delta+1)k + \lambda_n^2 D_{s,e} \right)^2 - 4k\lambda_n^2 D_{s,e}}}{2} \tag{23}$$

where for the sake of algebra we have set (see also Appendix A)

$$\delta = \frac{1-\varepsilon}{\varepsilon}.$$

The eigenvalues λ_n equal $\lambda_n = (2n+1) \cdot \pi/l$.

Observing Eqs. (19) and (20) we notice that process kinetics is determined entirely by the roots of the characteristic polynomial (given by Eq. (23)) of the hyperbolic equation (see Eq. A.15). If there is no electroporation and $k \to 0$, Eq. (23) can be simplified and gives $\gamma_{n,1} \to 0$ and $\gamma_{n,2} \to -\lambda_n^2 D_{s,e}$. At these conditions, diffusion kinetics is governed entirely by the rate of diffusion in extracellular space, i.e. $D_{s,e}$, and there is no transmembrane flow (since $k \to 0$). Eq. (1) becomes an ordinary one-dimensional diffusion equation, whose solution is well-known and can be found in e.g. [69]:

$$c_e(z,t) = \frac{4c_{e0}}{\pi} \sum_{n=0}^{\infty} \frac{(-1)^n}{2n+1} \exp\left(-\frac{D_{s,e}(2n+1)^2 \pi^2 t}{l^2} \right) \cos\left(\frac{(2n+1)\pi}{l} z \right). \tag{24}$$

We should point out however that the analytical solution given by Eqs. (19)–(20) becomes extremely unstable during numerical evaluation for $k \to 0$. As k decreases, numerical errors due to finite machine precision (32- or 64-bit floating point representation and operations) are amplified and the model results become unstable. For machine precision on the order of 10^{-16}, this effect becomes observable around $k = 10^{-13}$ and the results become completely unusable for $k < 10^{-14}$. At these extreme conditions however, there is no justification for use of the dual-porosity model whatsoever, and analysis of free diffusion in extracellular space is well described by a much simpler model, such as given by Eq. (24).

At the other extreme, for highly electroporated tissue ($f_p \to 1$), for f_p values above approximately 10^{-3}, the membrane appears to disintegrate, i.e. to lose its barrier function for solute diffusion. In Eq. (23) we

Table 1
Parameters used for model validation and the parametric study of the model.

Parameter	Symbol	Value
Diffusion coefficient − sucrose in water at 20 °C	$D_{s,0}$	4.5×10^{-10} m^2 s^{-1} [34]
Hydrodynamic radius of sucrose molecule	r_s	0.4 to 0.5×10^{-9} m [59,78]
Average stable pore radius	r_p	0.5×10^{-9} m [27,79]
Cell membrane thickness	d_m	5×10^{-9} m [80]
Long-lasting pore surface fraction ratio for one 100 μs pulse	f_p	1.4×10^{-6} [65]
Sucrose initial concentration[a]	c_{e0}, c_{i0}	1 mol m^{-3}
Volume fraction of cells	F	0.6 to 0.8 [71]
Diffusion coefficient of sucrose in extracellular space[b]	$D_{s,e}$	$D_{s,e} = D_{s,0}/\tau = D_{s,0} \cdot 2/\pi$
Average cell size (radius)	R	2.5×10^{-5} m [81]
Tissue sample size (cylinder radius)	ρ	0.0125 m
Tissue sample size (thickness)	l	0.002 m

[a] The absolute value of initial concentration is irrelevant for model analysis, since the model is linear and thus the resulting profiles of concentration kinetics are linearly scalable.
[b] Diffusion in extracellular space is assumed to occur at the rate of diffusion in water but reduced by the factor of tortuosity of the extracellular space. See the last paragraph of Subsection 2.1 for a detailed explanation.

then have $(\delta + 1)k >> \lambda_n^2 D_{s,e}$. This results in extremely fast kinetics ($|\gamma_2| \approx (\delta + 1)k >> 1$) of transmembrane transport and instantaneous diffusion of solute from the intracellular into the extracellular space, provided there is a concentration gradient. This is again unrealistic and outside the scope of the model, as the finite rate of intracellular diffusion is not captured by model equations. The other exponential however, $C_1 \exp(\gamma_1 t)$, is governed primarily by $D_{s,e}$, which limits diffusion out of the tissue block through the extracellular space. Since $C_1 >> C_2$ this results in almost identical diffusion kinetics in extracellular space as in non-electroporated tissue, but with comparatively higher concentrations at a given time. This is as expected, since the extracellular space has to facilitate vacation of not only the solute initially present in the extracellular phase, but of the solute present within the cells as well (determined by the initial condition for intracellular concentration).

As emphasized by this analysis, there are limitations of the proposed dual-porosity model and its analytical solution. These limitations must be kept in mind during experimentation with the model, and one should maintain a critical view at the results in light of these observations to avoid analysis under unrealistic or extreme conditions.

2.3. Parameters and experimental methodology for the model study of sugar extraction and the parametric study

To provide model validation, we performed diffusion experiments with sugar beet tissue pretreated with electroporation. The experimental setup was then modeled by the dual-porosity model and results were compared with experimental measurements. We also present a parametric study (see Results and discussion), by means of which we evaluate the sensitivity of the model to five parameters. Table 1 summarizes the parameters of the model that were used in the model study for validation of the model and for the (purely theoretical) parametrical study. The references are given in square brackets where applicable.

A brief note on the initial concentration; the parameters presented in Table 1 will be used for parametrical model analysis in the special case of plant tissue electroporation, and since we start observing diffusion in tissue about two to three minutes after the electric pulse application, we believe this pause is long enough to assume that initial concentrations inside and outside the cells are equal at the beginning of simulation. This initial state is supposed to result from release of intracellular fluid from electroporated cells containing solute of our interest (among other dissolved substances) into the extracellular space, a process that begins after applying electroporative pulses, presumably leading to local equilibrium in concentration before the start of the simulated diffusion experiment. Note that this supposition is only valid if

treatment is applied to the sample. In a non-electroporated sample, we would have to suppose an initial imbalance between the intra- and extracellular concentration.

The details of the experimental setup have been previously described elsewhere [22], though some important differences do exist in the particularities of the geometry and experiment execution. Cylindrical samples (disks) of sugar beet tissue were obtained from 5 mm thick sugar beet slices. The samples measured 25 mm in diameter. Each individual sample was electroporated by applying 400 V between parallel plate electrodes at 5 mm distance (sample thickness). Bipolar pulses rectangular in shape, of 100 μs duration each and pulse repetition frequency of 1 kHz were delivered within each train of 8 pulses. Two such trains were delivered with a pause of one second between the two trains. The samples were removed from the treatment cell, after which the surfaces of the disks were dried with absorbent paper to remove sugary liquid on the surfaces. This liquid is present due to cutting and possibly due to electro-osmotic or pressure-change effects that occur during the electroporation treatment. Note that had this step been omitted, the surface liquid would cause an immediate increase in sucrose concentration in the solution at the beginning of the experiment, an effect which is not captured by the model. The surface-dried samples were then placed into a flask with a magnetic stirrer. The liquid was constantly agitated and sampled at regular intervals; sucrose concentration was analyzed with a digital refractometer. The liquid-to-solid ratio was 2:1.

The quantity measured by the digital refractometer is sugar concentration in liquid with unit degrees Brix (°B). One degree Brix is 1 g of sucrose in 100 g of solution and represents the concentration of the solution as percentage by weight (% w/w). If we know the initial sugar content of the aqueous solution (°Bx$_0$) and the final content (°Bx$_d$) – which in an ideal situation would be equal to the total sugar content in a tissue sample – we can define *normalized degree Brix* at time t — i.e. $B(t)$, as

$$B(t) = \frac{°Bx(t) - °Bx_0}{°Bx_d - °Bx_0}.$$ (25)

Normalized Brix will be our measure for the amount of solute (e.g. sugar) that has diffused out of the tissue sample in time t. It takes the values $0 \leq B(t) \leq 1$ and is dimensionless. It is obtained by a trivial calculation from measurements with the refractometer, according to Eq. (25). To arrive at the same quantity from the spatio-temporal intra- and extracellular concentration profiles given by the model (see Fig. 7), these profiles must be integrated on the spatial coordinate z to obtain the observable and measurable bulk concentration of sucrose in

the solvent outside the tissue samples. The total mass left in the sample equals

$$m(t) = 2\pi\rho^2 \left[\varepsilon \int_0^{l/2} c_e(z,t)dz + (1-\varepsilon)\int_0^{l/2} c_i(z,t)dz \right]. \tag{26}$$

On the other hand, the total initial mass of solute is equal to

$$m_0 = m(0) = \pi\rho^2 l[\varepsilon c_{e0} + (1-\varepsilon)c_{i0}]. \tag{27}$$

Normalized Brix for the solution into which the sample is submerged is then

$$B(t) = 1 - \frac{m(t)}{m_0} = 1 - \frac{2\left[\varepsilon \int_0^{l/2} c_e(z,t)dz + (1-\varepsilon)\int_0^{l/2} c_i(z,t)dz \right]}{l[\varepsilon c_{e0} + (1-\varepsilon)c_{i0}]}. \tag{28}$$

A subtraction of $m(t)/m_0$ from 1 is necessary since we are interested in the extracted solute and not the amount remaining in the sample.

2.4. The dual-porosity model of tissue electroporation in biomedicine — model generalization

To demonstrate the universal applicability of the dual-porosity model in modeling tissue electroporation, we describe in this section the necessary modifications to the model that are required to study transport phenomena in two biomedical applications of electroporation: electrochemotherapy (ECT) [10], and trans- or intradermal drug transport [16].

The objective of ECT is to facilitate introduction of chemotherapeutic drugs into tumor cells by applying electroporation [82]. The two most commonly used drugs in ECT are bleomycin and cisplatin. Bleomycin is a highly potent drug that binds to DNA where it causes DNA cleavage resulting in eventual cell death at mitosis; it however poorly permeates the intact cellular membrane. Electroporation enhances the drug uptake and thus low local or systemic drug concentrations can be used for effective local chemotherapy. As a model example, we examine the situation illustrated by Fig. 5. The subcutaneous tumor is modeled as an oblate spheroid embedded into the subcutaneous tissue immediately under the skin layer. In this model configuration, the tumor is separated from the surrounding tissue by two interfaces; the tumor–subcutaneous tissue boundary surface and the tumor–skin boundary surface. For the purposes of further analysis, we establish the following set of assumptions: a) In our example, bleomycin is given intravenously, not intratumorally. Due to interstitial fluid pressure that is present inside the tumor before electroporation [83,84], the initial drug concentration inside the tumor region for both intra- and extracellular spaces is zero, as the drug cannot extravasate into the tumor region; b) If surface-applied plate electrodes are used, the skin is electropermeabilized along with the tumor, the resulting vascular lock [85,86] and damage due to irreversible electroporation in the dermis warrant the supposition that skin presents a negligible sink or source of bleomycin, i.e. from the point of view of pharmacokinetics, the skin does not represent a compartment; c) Provided the perfusion of subcutaneous structures remains unaffected by electroporation, it can be represented, locally, as an infinite reservoir of bleomycin, since the localized drop in concentration due to cellular uptake is immediately replenished via convective transport by the vascular system; d) If the drug has difficulties entering tissue (e.g. due to interstitial fluid pressure), its concentration locally may be low within the tumor region. In those areas, bleomycin that is reacting with the DNA and is getting used up decreases the drug concentration, which may be important. We thus include in the model the bleomycin reaction rate R_B, where $R_B < 0$; e) Achieving local tumor coverage with

fields above the threshold of reversible electroporation is critical for permeabilizing the cells and facilitating bleomycin uptake. Electrode configuration, placement, pulsing protocol, and tissue electrical properties determine field distribution and the energy delivered. These factors should not be neglected as the research field is highly advanced on this subject and importance of local field distribution has been strongly emphasized in numerous works, see e.g. [87–89].

The model equations for tumor intra- and extracellular concentrations c_i and c_e, respectively, are

$$\frac{\partial c_i}{\partial t} + k(c_i - c_e) - R_B = 0 \tag{29}$$

$$\frac{\partial c_e}{\partial t} + \nabla \cdot \left(-D_{B,e}\nabla \cdot c_e \right) - \frac{1-\varepsilon_t}{\varepsilon_t}k(c_i - c_e) = 0 \tag{30}$$

where $D_{B,e}$ is the bleomycin diffusion coefficient in the extracellular space and ε_t is the porosity of tumor tissue. Note that in Eqs. (29)–(30) the concentrations are functions of all 3 spatial coordinates and time. R_B is the reaction rate of bleomycin as it binds to DNA. There is also a difference in the flow coefficient k as compared to the expression previously given by Eq. (8). In Eqs. (29)–(30) above,

$$k(t,E) = \frac{3D_{B,eff}f_p(t)}{d_m R} \cdot u(E) \tag{31}$$

where

$$u\left(\left| E\left(\vec{r}\right)\right|\right) = \begin{cases} 1 & ; \left| E\left(\vec{r}\right)\right| > E_{rev} \\ 0 & ; \left| E\left(\vec{r}\right)\right| < E_{rev} \end{cases}. \tag{32}$$

The introduced function $u(E)$ is a unit step that models the effects of the inhomogeneous electric field established in tissue and is a time-invariant function of local maximal electric field strength distribution. E_{rev} is the reversible field strength threshold (scalar value) that must be reached locally to successfully permeabilize the cells [61,90]. Additionally, the pore surface fraction f_p of long-lasting pores is now time-dependent to capture the effects of pore resealing [59]. Due to the interstitial fluid pressure within the tumor (see model assumption a), initial conditions are:

$$c_{i0} = c_i(t=0) = 0 \tag{33}$$

$$c_{e0} = c_e(t=0) = 0 \tag{34}$$

and boundary conditions (according to model assumptions b and c) are

$$[c_e]_{S_1} = c_e^{\,s}(t) \tag{35}$$

$$\left[\frac{\partial c_e}{\partial \vec{r}}\right]_{S_2} = 0 \tag{36}$$

$$\left[\frac{\partial c_i}{\partial \vec{r}}\right]_{S_1} = \left[\frac{\partial c_i}{\partial \vec{r}}\right]_{S_2} = 0 \tag{37}$$

where S_1 is the tumor–subcutaneous tissue boundary surface and S_2 the tumor–skin boundary surface (see Fig. 5). For intracellular bleomycin concentration, both boundaries are reflective (no-flux), while for the extracellular concentration the tumor–skin boundary surface is reflective and the tumor-subcutaneous tissue boundary surface has a prescribed time-dependent concentration $c_e^s(t)$. This is the extracellular concentration of bleomycin in the subcutaneous
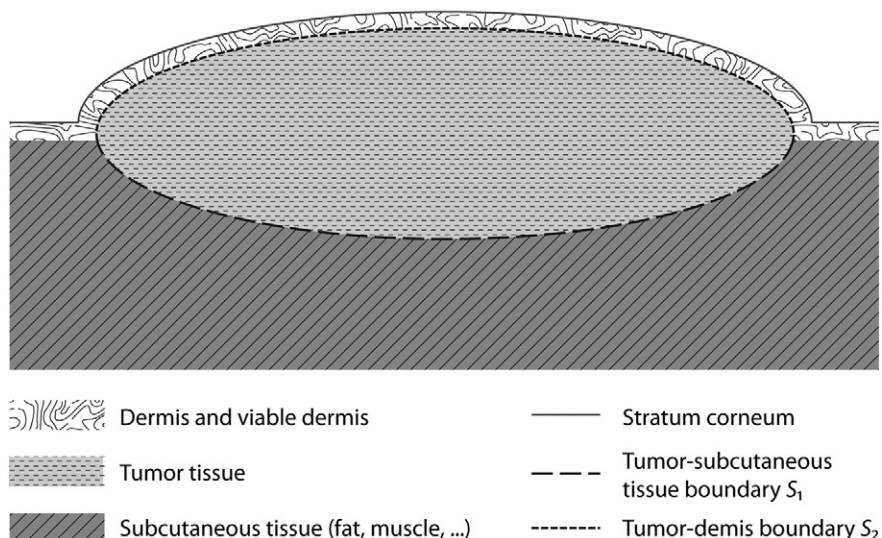
Fig. 5. Model of a subcutaneous tumor.

tissue (comprising fat and muscle tissue, and the vascular system) and is determined by the amount of drug given intravenously, the body mass of the animal and the time passed since the moment of injection. Solving the system of Eqs. (29)–(37) is out of the scope of this paper and requires a numerical approach. Finite element software supporting immediate and direct implementation and analysis of this exemplary model is readily available on the market (e.g. COMSOL Multiphysics, COMSOL AB, Sweden).

In the second example of applying the dual-porosity model in the biomedical field we examine the trans- and intradermal drug transports [16]. For transdermal drug transport, perhaps the most interesting effect of electroporation application to the skin is the disruptive effect of electric pulses to the skin's most protective barrier layer — the stratum corneum (SC). Due to formation of the so-called local transport regions (LTRs) [14,15] during electroporation, the permeability to molecules of the skin's outermost protective layer can be increased by orders of magnitude. During electroporation, this occurs rather rapidly and as subsequently the electrical resistance of the SC drops, this allows for electroporation of underlying skin layers (see Fig. 6). The disruption of the barrier function in SC facilitates diffusion of molecules with molecular weight even greater than 7 kDa, though the process is

relatively nonspecific and dose control difficult [16]. To enhance the passive transport, application of low-voltage electrophoretic pulses after high-voltage electroporation has been proposed and is a subject of recent studies [91]. If the therapeutic molecules (e.g. DNA material, or fentanyl [92]) are present in the dermis, electroporation facilitates uptake of these molecules by viable electroporated cells of the dermis and/or underlying tissues [16]. This is the intradermal application, used, in example, for intradermal gene transfection for DNA vaccination [93]. Given the structure of the skin (stratum corneum, viable epidermis, dermis, follicles, etc.) there are several routes available for transport. Which route is more important depends on the treatment protocol and the properties of the drug (charge, size, partition coefficient). In example, lipophilic molecules can permeate via the transcellular route, while hydrophilic molecules generally do not. If the epidermal cells are electroporated however, the hydrophilic molecules can enter the cells of the epidermis with expressed therapeutic effect.

To model this situation with the dual-porosity model, we examine the situation conceptualized with the help of Fig. 6. A patch (reservoir) containing the therapeutic drug is placed on the electroporation-treated section of the skin, and we are interested in the amount of
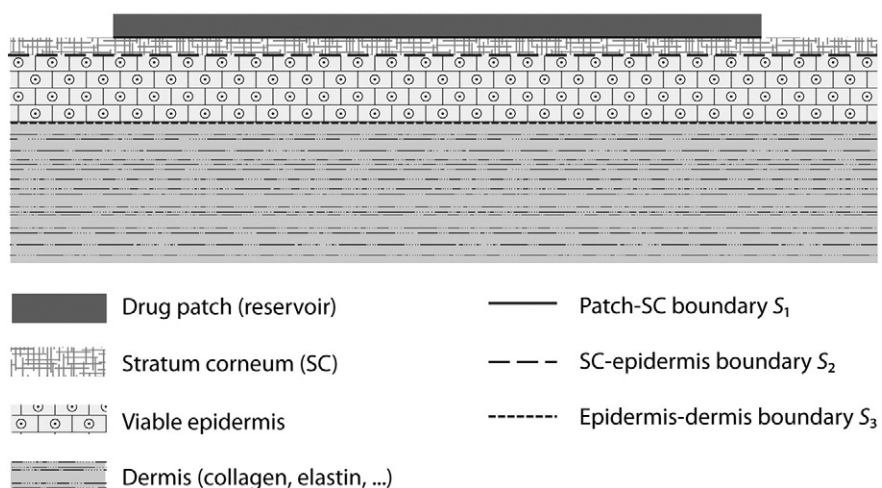

Fig. 6. The conceptual skin model for the transdermal drug delivery example.

drug reaching the bottom-most layer, i.e. the basal layer, of viable epidermis. Following the model of SC permeabilization established by Becker [15], we write, for the SC layer,

$$\frac{\partial c^{SC}}{\partial t} = \frac{1}{\tau_{SC}} \left[\nabla \cdot \left(D_L \nabla c^{SC} \right) \right] \tag{38}$$

where c^{SC} is the intrinsic (not accounting for porosity!) drug concentration in the lipid pathways between corneocytes in the SC and τ_{SC} is the tortuosity of the SC phase. D_L is the effective diffusion coefficient of the permeating drug in the porous lipid-filled spaces between the corneocytes in the SC layer. Assuming the SC layer is homogeneous and the patch containing the drug as well as the electroporated area are large as compared to the thickness of the SC layer, only the gradient along the principal axis of diffusion can be considered and diffusion coefficient moved out of the gradient operator, yielding

$$\frac{\partial c^{SC}}{\partial t} = \frac{D_L}{\tau_{SC}} \frac{\partial^2 c^{SC}}{\partial z^2} \tag{39}$$

with initial condition $c^{SC}(z, 0) = 0$, and boundary conditions

$$\left[c^{SC} \right]_{S_1} = c_R(t) \tag{40}$$

$$\left[c^{SC} \right]_{S_2} = \left[c_e^E \right]_{S_2} \tag{41}$$

$$\left[\frac{\varepsilon_{SC} D_L}{\tau_{SC}} \frac{\partial c^{SC}}{\partial z} \right]_{S_2} = \left[\frac{\varepsilon_E D_E}{\tau_E} \frac{\partial c_e^E}{\partial z} \right]_{S_2} \tag{42}$$

where ε_{SC} is the porosity of the SC layer, ε_E and D_E are the porosity and effective drug diffusion coefficient in the epidermis, respectively, c_R is the reservoir (drug patch) concentration that can be modeled as constant if the drug is poorly permeable and the reservoir volume large, c_e^E is the epidermis extracellular intrinsic concentration, and τ_E is the tortuosity of the lipid-filled pathways in the epidermal layer. If the cells of the epidermis are electroporated and this significantly influences the drug's ability to enter viable cells, we can now write the dual-porosity model equations for the epidermis

$$\frac{\partial c_e^E}{\partial t} - \frac{D_E}{\tau_E} \frac{\partial^2 c_e^E}{\partial z^2} - \frac{1-\varepsilon_E}{\varepsilon_E} k_E \left(c_i^E - c_e^E \right) = 0 \tag{43}$$

$$\frac{\partial c_i^E}{\partial t} + k_E \left(c_i^E - c_e^E \right) - R_d = 0 \tag{44}$$

where c_i^E is the epidermis intracellular intrinsic concentration, R_d the reaction rate of the drug species d as it reaches its intracellular target, and k_E the epidermis permeabilization coefficient calculated according to Eq. (8). The rest of the boundary conditions, in addition to Eqs. (41)–(42) are all homogeneous Neumann (i.e. no-flux) boundaries

$$\left[\frac{\partial c_i^E}{\partial z} \right]_{S_2} = \left[\frac{\partial c_i^E}{\partial z} \right]_{S_3} = \left[\frac{\partial c_e^E}{\partial z} \right]_{S_3} = 0 \tag{45}$$

and initial conditions are $c_e^E(z, 0) = c_i^E(z, 0) = 0$.

If the finite dimensions (capacity) of the drug patch are not negligible, i.e. the emptying of the reservoir is significantly fast due to high rate of trans- or intradermal diffusion, we have to account for the fact the patch concentration of drug c_R is time-dependent. In this case, the concentration c_R can be expressed according to the law of mass conservation as

$$c_R(t) = c_{R0} - \frac{D_{SC}}{d_R} \int_0^t \frac{\partial c^{SC}}{\partial z}\Big|_{S_1} dT \tag{46}$$

where d_R is the thickness of the patch or more precisely, the patch volume to SC-patch contact surface ratio, D_{SC} is the effective drug diffusion coefficient where the complete SC layer is taken into account ($D_{SC} = D_L \varepsilon_{SC}/\tau_{SC}$), and c_{R0} is the reservoir initial drug concentration.

The two examples given above illustrate how the dual-porosity model can be incorporated into or coupled with existing models developed within their respective fields of biomedical electroporation applications. Further development of these models, parameter estimations and validation extend beyond the scope of this paper and are the subject of our future work.

3. Results and discussion

3.1. The intra- and extracellular concentration profiles — visualization of model results

All of the following figures were made with MATLAB version 2012a (MathWorks, Massachusetts, USA), an engineering software package by means of which the analytical solution was implemented in computational terms, and built-in functions provided by this package were used to draw the calculated results. The meshing coefficient (number of vector elements for space and time) was 100 in all cases, providing good spatial and temporal resolutions. Fig. 7 presents the extracellular (Fig. 7a, c) and intracellular (Fig. 7b, d) concentrations as a function of space and time, obtained via the analytical calculation for the set of parameters presented in Table 1 (upper limit values were used where a range is given). In terms of the spatial dimension, only one half of the tissue slab is modeled since we have assumed symmetry along the central plane (see Fig. 3). We can observe (Fig. 7a, b) that while in intact tissue solute diffuses out of the extracellular space and into the space surrounding the tissue block relatively unhindered at a rate determined by $D_{s,e}$, it is mostly retained in the intracellular space. This is consistent with observation, since the surface fraction ratio of pores close to 1.4×10^{-6} corresponds to a single 100 μs pulse of amplitude that is generally considered insufficient to successfully permeabilize the membrane [49,65,94].

Fig. 7c–d shows the results for a situation very similar to that illustrated in Fig. 7a–b, but with a change in one model parameter. To obtain results given by Fig. 7c–d, we have made an increase in value of f_p from 1.4×10^{-6} to 2.5×10^{-5}, effectively increasing the pore surface fraction (and thus k) by about an order of magnitude. As a result, solute diffuses noticeably from both the intracellular space as well as the extracellular space. Notice that the extracellular concentration at the end of the simulation (7200th second, Fig. 7d) is higher than the corresponding concentration in Fig. 7a due to the contribution of intracellular solute diffusing out of the cells.

Fig. 8 shows intracellular intrinsic concentration calculated analytically for $n = 0$ (Fig. 8a), $n = 0...3$ (Fig. 8b) and $n = 0...10$ (Fig. 8c) for the same set of parameters used to obtain Fig. 7d, where n is the index of the infinite series in Eqs. (19)–(20). Fig. 8 demonstrates rapid convergence of the series given by Eq. (19). If we look carefully at Fig. 8a, we may observe a slight overestimate of concentration near $z = 0$, which is almost completely gone if we account for 4 members of the series (Fig. 8b) and for even higher accuracy, becomes impossible to detect by merely examining concentration profiles, as is evident in comparing Fig. 8b and 8c. This rapid convergence makes the analytical model highly suitable for use in optimization algorithms, in which optimal values of parameters may be determined given a set of experimentally-obtained data. Note that the boundary condition for extracellular concentration in combination with constant initial condition
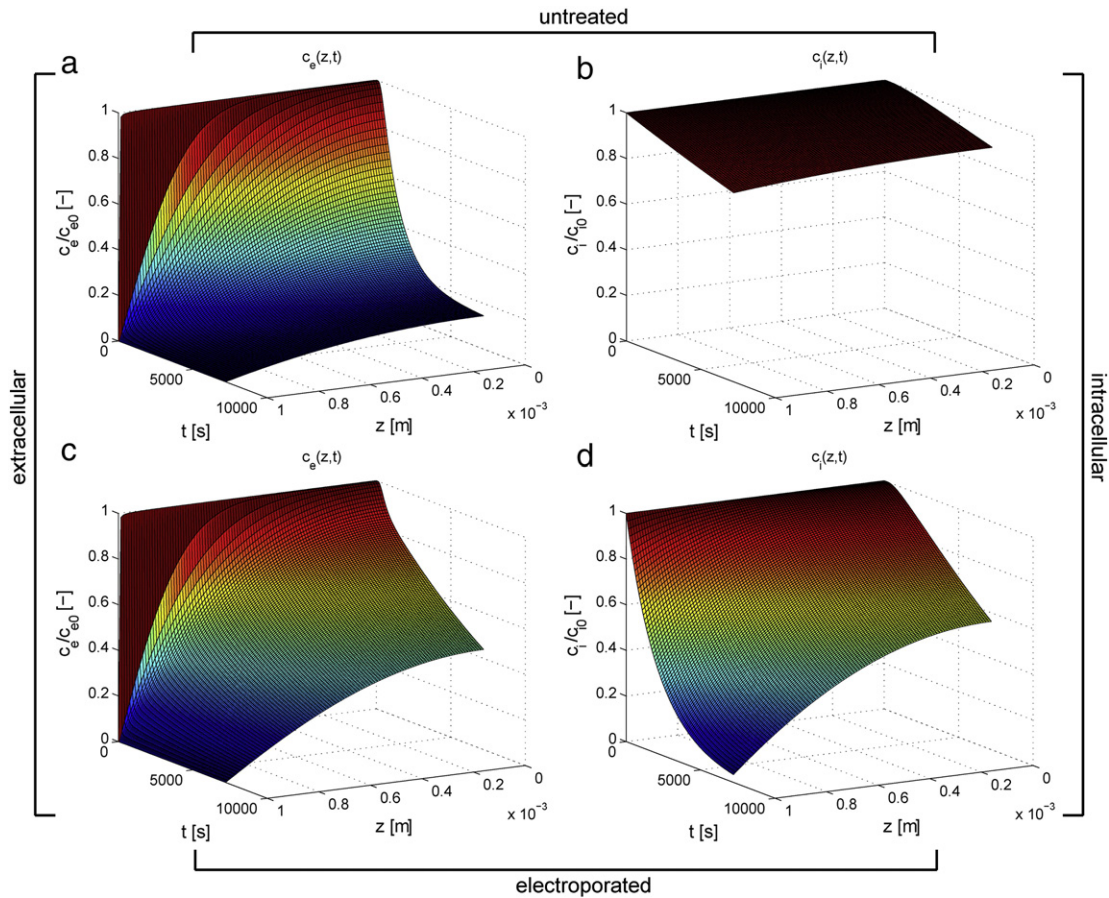
Fig. 7. Results of the calculation of concentration in our model study for parameters given in Table 1. The spatio-temporal dependence of intrinsic concentration in the extracellular (a) and in the intracellular space (b) for one 100 μs pulse (almost intact tissue). Results after increase of the pore surface fraction f_p by about one order of magnitude; extracellular (c) and intracellular (d) intrinsic concentration.

(an artifact of modeling only for the steady-state conditions) results in a sharp discontinuity at $z = l/2$. This makes the series in Eq. (20) converge rather poorly. To overcome this limitation, we calculate intracellular concentration first according to Eq. (19), then perform (numerically) differentiation, multiplication and addition according to Eq. A.1 (see Appendix A) to obtain extracellular concentration, avoiding the use of the poorly convergent infinite series (Eq. (20)) altogether.

3.2. Model study with extraction experiments — model validation

In this section we evaluate how well the described model performs at the task of modeling a particular process and explaining

experimentally obtained data. The details of the experiment have been previously described in the literature [22]. Important deviations from the published setup were described in Section 2.3 of this paper. Data obtained during the course of these experiments was used for the purposes of the following analysis.

In the experiments, cylindrical blocks of sugar beet tissue were pretreated with electric field according to a protocol ensuring a low degree of membrane permeabilization (see section 2.3). Following the electroporation treatment, samples were placed into a diffusion chamber. In the literature where such or similar experiments have been described, quantitative analysis of the results is often done by fitting the experimental data to the model of diffusion kinetics in a
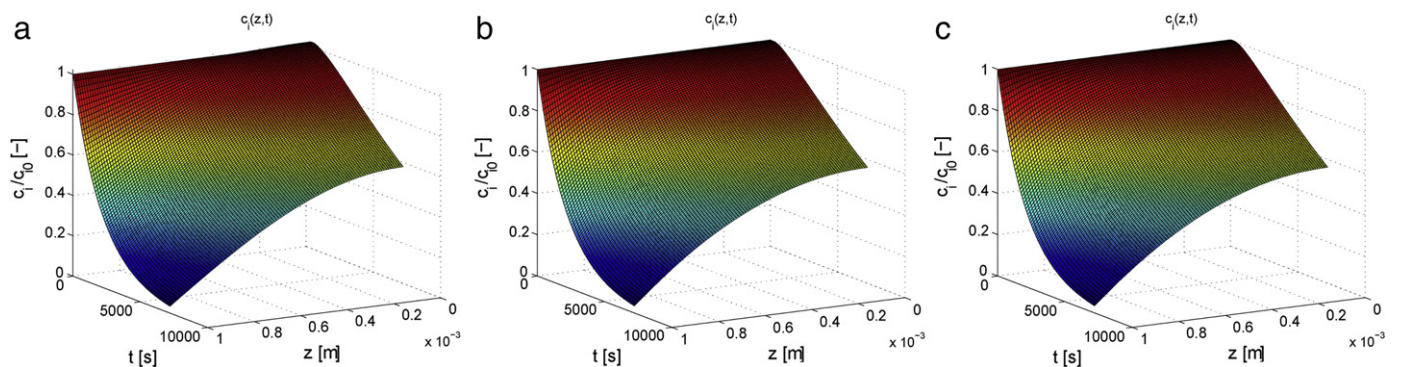
Fig. 8. Analytical solution for intracellular concentration according to the dual-porosity model. (a) For $n = 0$ (see Eq. (19)); (b) for $n = 0...3$; and (c) for $n = 0...10$.

homogeneous plane sheet of uniform thickness, found in e.g. [69] and obtainable by integration of Eq. (24) (see section 2.2). The normalized Brix according to this model is

$$B = 1 - \frac{8}{\pi^2} \sum_{n=0}^{\infty} \frac{1}{(2n+1)^2} \exp\left(\frac{-D_{\text{eff}}(2n+1)^2\pi^2 t}{l^2}\right) \qquad (47)$$

where l is, contrary to the definition in [69], the total sample thickness (not half-width) as defined and used in this paper. Note that D_{eff} in Eq. (47) is the effective diffusion coefficient in the (homogeneous!) material forming the plane sheet, and must not be confused with the effective pore diffusion coefficient $D_{\text{s,eff}}$ as defined earlier in this paper. As the series in Eq. (47) converges rapidly for large values of time, about five of the first members of the series are usually accounted for to find the effective diffusion coefficient by fitting the model to the experiment with the least-square error method. In doing so however due to the nature of the one-exponential model we sacrifice a good fit for either low or for high values of time. In Fig. 9, we show experimental data and three results of modeling. Two were obtained using Eq. (47) and the third is a result of parametrical optimization on the dual-porosity model. From comparison of all three model results (RMSD equal to 0.173 and 0.092 for model in Eq. (26) using $D_{\text{eff}} = 0.15 \times 10^{-10}$ and $D_{\text{eff}} = 0.34 \times 10^{-10}$ m^{2}s^{-1}, respectively; and to 0.014 for the dual-porosity model) it is evident that the dual-porosity model provides for a superior fit and can explain what the one-exponential model of homogeneous material cannot; that is the approximately linear increase in sucrose concentration during the experiment (except at the very beginning), as a result of hindered diffusion of the sucrose deposited in the intracellular space leaving the tissue block via the extracellular route. The model as given by Eq. (47) is insufficient to capture this phenomenon as it has been derived for a sheet of homogeneous material with one effective and constant rate of diffusion (governed by D_{eff}). The dual-porosity model however offers this possibility since its temporal solution is based on a description of the system via a 2$^{\text{nd}}$ order hyperbolic differential equation (see Appendix A). This means we have, in terms of kinetics, two additive exponential members in the solution determined by the parameters of electroporation and its impact on the porosity of the membrane separating the two phases. According to the theory of electroporation and our understanding of its effects on cells

in tissue, such a model is needed to capture the contribution of presumably faster extracellular diffusion and that of slower, hindered diffusion, out of electroporated cells through a semi-permeable membrane. What is even more important is that the effective diffusion coefficient as obtained from fitting experimental data by Eq. (47) has no physiological meaning. It is purely phenomenological, as it does not equal either the rate of extracellular diffusion, neither the rate of transmembrane diffusion, nor the solute diffusion coefficient in the liquid medium (i.e. water). On the contrary, all of the parameters used in the dual-porosity model reflect properties of the tissue before or after electroporation treatment. The parameter values are either obtained from or estimated based on published literature.

A note about the method used for initial estimation of f_p, the fraction of long-lived pores, used to model experimental data as shown in Fig. 9. Table 1 gives f_p determined based on experiments as described in [65], where the authors give an estimation of the fraction of long-lived pores for a single 100 μs pulse of 860 V/cm, as well as a train of 2, 4 and 8 such pulses. Since we used a similar protocol, applying 800 V/cm in two trains of 8 pulses (details can be found in Section 2.3), we linearly extrapolated the results of the cited study, and we arrived to an initial estimate for pore surface fraction on the order of 10^{-5}. However, via model simulation and optimization of results to match the experimental data, we had to reduce this estimate by 10% to 0.9×10^{-5}, in order to obtain the best agreement between the model and the experimental results.

Also note that since the experimental data used to evaluate the model in this specific example was obtained at a relatively low degree of membrane electroporation (disintegration index Z [38] equal to about 0.35), the potential for quantitative analysis of this model cannot be accurately assessed from a single experimental study alone. The low degree of permeabilization also results in a higher discrepancy between the dual-porosity model results and results of the model of homogeneous material, thus demonstrating the better performance of the dual-porosity model under such conditions. During experiments at various treatment intensities (pulse number and duration) we observed that as tissue is being treated by electroporation of ever increasing intensity, it also tends to behave more and more as though it were a homogeneous material. Thus, further work is needed in order to evaluate the model in relation to experimental results, especially at higher degrees of membrane electroporation.

### 3.3. Parametrical study — analysis of model behavior and sensitivity

We begin by analyzing the influence of pore surface fraction, f_p. Fig. 10a gives $B(t)$ for a number of values of this parameter, equally spaced on a logarithmic scale. We observe that for very low values of pore surface fraction, B reaches the value 0.2, which is the volume fraction of extracellular space used in this model study (Table 1). This makes sense, as only the solute present in the extracellular medium is extracted. For highly porous membranes on the other hand, the final B is just below 0.7, a consequence of simulation time which is not long enough (relative to the extracellular diffusion rate and sample dimensions) to allow for all the solute to vacate the tissue sample completely (see Fig. 7). In between these two extremes, the total yield of solute at simulation end changes rapidly for pore surface fractions between 10^{-6} and 10^{-4}. This is clearly demonstrated in Fig. 10b, where the value of B at simulation end is plotted for sixteen (arbitrarily chosen number) distinct values of f_p in the range $2.5 \times 10^{-10} \leq f_p \leq 7.5 \times 10^{-3}$.

Next, we analyze the impact of varying λ_r, the solute to pore radius ratio. This is perhaps the most difficult and problematic of the parameters of the model we present, since it displays a strong nonlinearity (see Eqs. (10)–(11) and Fig. 4) and very rapidly approaches 0 as the radius of solute becomes comparable to the radius of an average pore, which is our case since the sucrose hydrodynamic radius of about 0.4 nm is
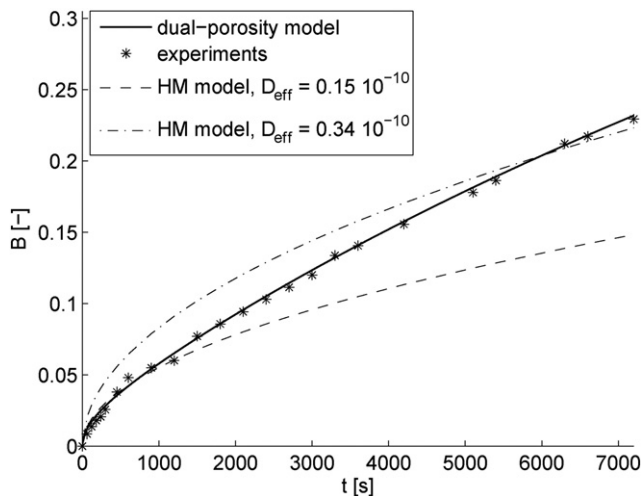
Fig. 9. Fitting the model to experimental data. The experimentally obtained data and the best-fit dual-porosity model results are given along with two plots of Eq. (47) using different value of parameter D_{eff}. The two values were selected in order to obtain a good agreement either during the initial 1000 s or towards the end of the experiment. Parameters of the dual-porosity medium used (those that differ from Table 1): $f_p = 0.9 \times 10^{-5}$, $l = 0.005$ m. HM in figure legend stands for homogeneous material.
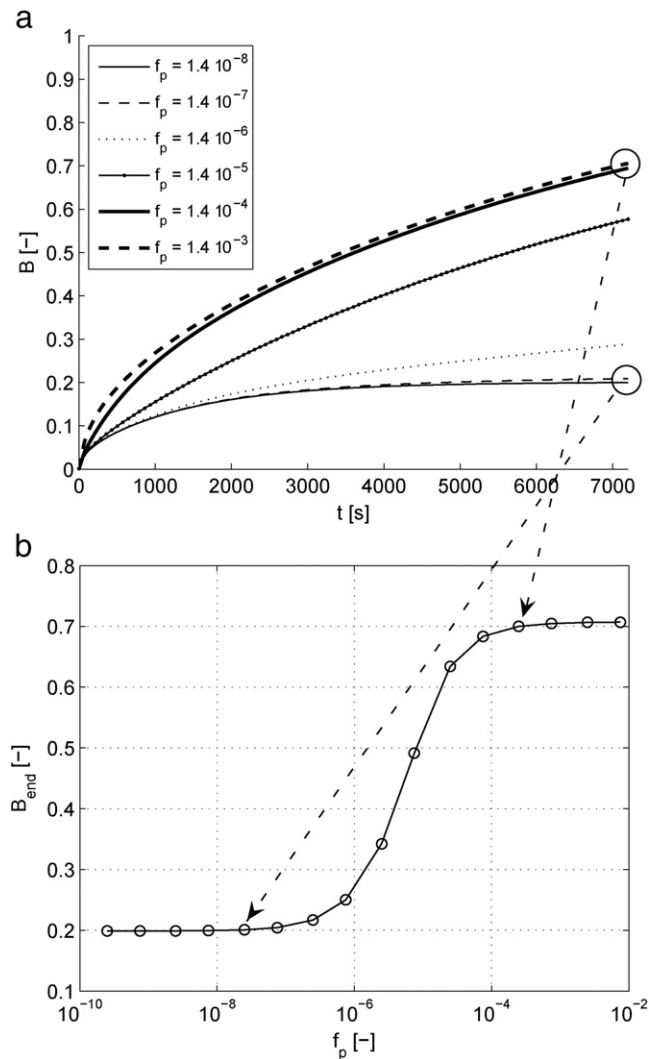
Fig. 10. (a) Normalized Brix as a function of time for six distinct values of pore surface fraction. (b) Normalized Brix at the end of simulation for sixteen values of pore surface fraction − note the sharp increase around $f_p = 10^{-6}$.

comparable to a 0.5 nm radius of a stable electro-pore. Often the solute radius is unknown and pore size is hard to determine, but even at best it is always a result of a statistical model or estimation based on particular experiments. The value used in this study ($\lambda_r = 0.85$) is based on rough estimates of both the solute and average pore size from literature and should be understood as a best guess that enables this model to present results and the parametric study consistent with literature. A detailed analysis and development of the model in this direction are matters of future research. The impact of λ_r on the effective pore diffusion coefficient is already given in Fig. 4. We varied this parameter linearly within the range $0.05 \leq \lambda_r \leq 0.95$ and the effect on normalized Brix is shown in Fig. 11a.

In Fig. 11b we examine the impact of volume fraction ratio of cells in tissue *F*, as defined in section 2.1 (see model assumptions). The fraction ratio is very important for extraction dynamics since it defines the porosity of tissue ε (where $\varepsilon = 1 - F$), and porosity determines the macroscopically observable rate of diffusion, as viewed within the context of the complete block of tissue. If rate of diffusion is averaged over the entire volume of the tissue sample, the extracellular diffusion coefficient is dependent on the extracellular porosity, $D_{s,e} = \varepsilon/\tau \cdot D_{s,0}$, and thus on the volume fraction of cells in tissue. However, the effects of electroporation on these parameters, or indeed on the porosity, are not well known and will have to be evaluated in the future. We have

included this parameter in the analysis, since experimental and theoretical evidences exist that the cell volume fraction ratio is a function of electroporation [95,96]. The effective change (an increase) of cell volume ratio has been observed to occur in animal tissues due to colloid-osmotic swelling [95] and presumably cell shrinkage in plant tissue due to loss of turgor [96] during and after electroporation causes an effective decrease of the cell volume fraction. Moreover, with very high degrees of damage to tissues in extraction processes, a fraction of cells may be irreversibly electroporated. Irreversible electroporation leads to cell lysis, and we can reasonably assume that after the complete loss of the barrier function of the cell membrane, we can no longer consider the space previously occupied by the cell as intracellular space. We also need to consider that cell volume fraction ratio is dependent on the tissue sample and origin, as it varies between species of animal or plant whose tissue we are subjecting to the electroporation treatment. Plant tissues, in example, exhibit various volume fractions by virtue of natural diversity alone, among different species and even samples taken from a single species, depending on growing, harvest, and storage conditions [71].

Since some of the processes in electroporation-facilitated mass transfer also occur at temperatures higher than room temperature, e.g. in extraction of compounds from plant tissues, a combination of electroporation and temperature as high as 80 °C is used [22,97] and for clinical electrochemotherapy the temperature is that of the patient's body, we present model results at different temperatures by means of varying the diffusion coefficient $D_{s,0}$ (see Fig. 11c). The diffusion coefficient at various temperatures was recalculated from measurements reported in the literature [34] with the help of the Einstein–Stokes relation and data on viscosity of water as a function of temperature [98].

Fig. 11d shows the influence of the more realistic assumptions about initial extracellular concentrations for low degrees of membrane permeabilization. To obtain Fig. 10a, we assumed that initial intrinsic concentrations are equal in the extracellular space and the intracellular space, i.e. $c_{i0} = c_{e0}$. The rationale is that since some time passes between the electrical treatment of a sample and the beginning of a diffusion experiment, for high degrees of electroporation the intra- and extracellular concentrations equilibrate. At low permeability of the cell membrane however, this assumption is no longer valid. We therefore illustrate extraction kinetics if at $f_p = 1.4 \times 10^{-6}$ the c_{e0}/c_{i0} ratio varies within the range [0.2, 1].

Notice that λ_r (Fig. 11a) does not dramatically decrease the speed of diffusion at around the value of 0.20, but has a very strong impact at values of 0.45 and above, where the transmembrane through-pore flux due to constriction is brought almost to a halt. This is explained by the highly nonlinear relation between λ_r and the effective diffusion coefficient, as previously shown by the insert in Fig. 4. An interesting point is made by interpreting the results at very low values of λ_r. Under these conditions, we have low permeabilization ($f_p = 1.4 \times 10^{-6}$) but a high yield of solute that has diffused out of the tissue. We can suppose the transport modeled at these parameter values is that of small molecules (much smaller than sucrose) and that of ions.

Not surprisingly, the dependence on volume fraction of cells (Fig. 11b) shows a linear dependence on extracted solute yield due to low pore surface fraction used in simulation (see Table 1), resulting in the bulk of diffused (extracted) solute being the solute found initially in the extracellular medium.

Results in Fig. 11c quantify the effect of increasing the temperature of extraction if only the thermal effects on diffusion rate are supposed, with no influence of heat on cell or tissue structure. The values of $D_{s,0}$ used correspond to 20, 30, 40, 50, 60 and 80 °C.

The model results given by Fig. 11d confirm our expectations and are in accordance with performed diffusion experiments (as published in the literature, see e.g. [22]). If membrane permeabilization is low or nil, only extracellular sucrose diffuses and as the sucrose is primarily stored in the intracellular vacuoles, the final yield is low. Note that the range of values on the ordinate axis is [0, 0.5].
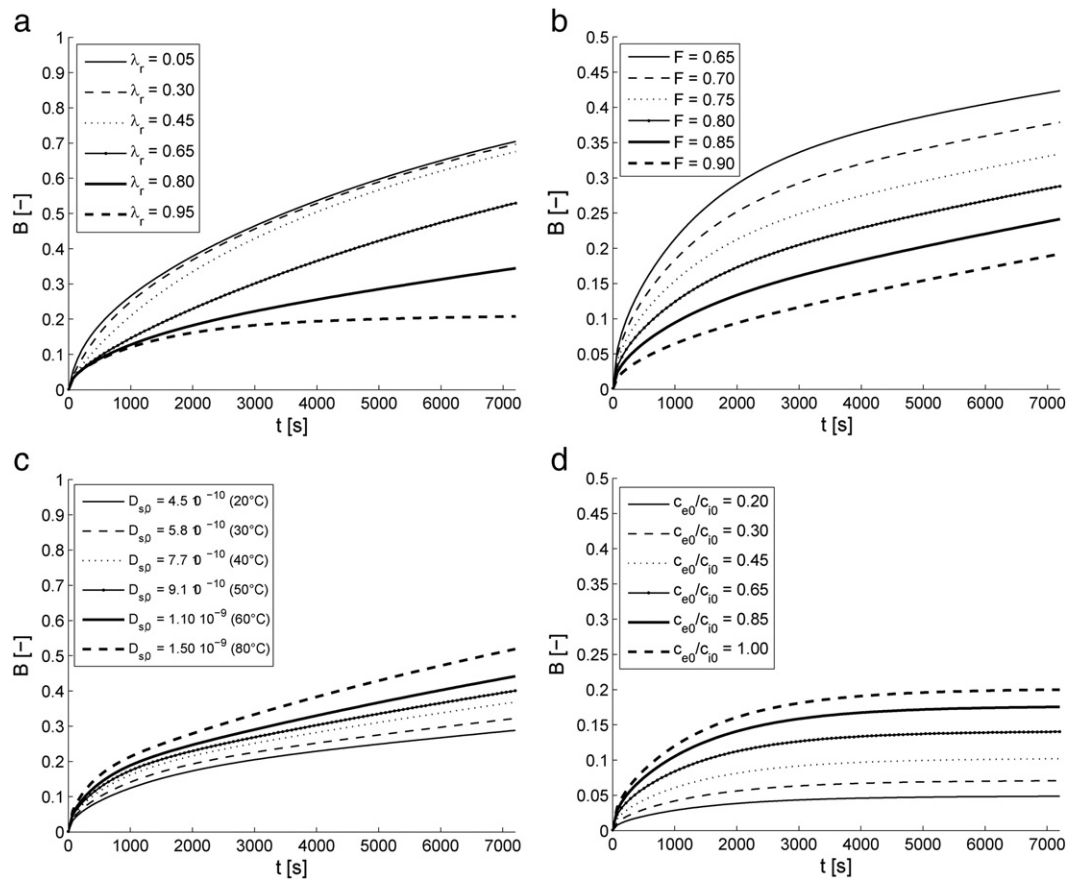
Fig. 11. Parametrical analysis of the model. (a) Varying the solute to pore radius λ_r. (b) Varying the cell volume fraction F. (c) Effect of temperature through its influence on diffusion coefficient of sucrose. (d) Varying c_{e0}/c_{i0} at no membrane permeabilization, i.e. $f_p \approx 10^{-8}$.

4. Conclusions

This paper gives an account of the development of a dual-porosity model of solute diffusion in tissue treated with electroporation. The fundamental assumptions in developing this model are based on phenomenological observations of liquid flow in porous media such as fractured rocks and soils. The model is designed as an attempt to provide a framework for future work in both computer modeling and experimental design. We demonstrated how it can be applied to a typical problem of solute extraction by diffusion in tissue that has been pretreated with electroporation, and we illustrated how it can be adapted to model mass transport phenomena in a disparate field of biomedical electroporation applications. We are confident that the dual-porosity model can be further improved and adapted to solve problems in mass transfer in many applications of electroporation, whether we are observing animal or plant tissue, whether we are interested in extraction of solute from the cells or introduction of solute into the cells, and even whether our species of interest are small ions or large organic compounds. The basic physical phenomena underlying the processes after application of electroporation treatment exhibit differences predominantly in details, which renders a general approach such as described by this paper, possible. The main focus of future work on the model will be verification by further experimentation, consolidation, as well as further inquiry designed to determine the influence of four important factors: pore evolution in number and size as a function of time; solute diffusivity through permeated membrane with pores evolving according to a model of electroporation; effect of net electric charge of solute and the effects of electroosmosis and electrophoresis; and the impact of electrical

tissue damage to the effective cell volume fraction and consequent effect on the porosity of biological tissue, which influences the rate of solute diffusion within the extracellular phase. The model is easy to adapt and extend and can be thus further enhanced, albeit at the cost of losing the possibility of obtaining an analytical solution and having to solve the model numerically.

Acknowledgements

Appendix A. Derivation of the analytical solution for constant coefficients k and $D_{s,e}$

In this Appendix we give a complete and detailed derivation of the analytical solution, given by Eqs. (19)–(23) in the main body of the paper, as it is derived from model Eqs. (1)–(2) taking appropriate initial and boundary conditions (Eqs. (12)–(18)) into the account.

We begin by joining the two first-order PDEs, Eq. (1)–(2), into one second-order PDE for solute concentration in intracellular space. From Eq. (2), we express c_e as

$$c_e = \frac{1}{k}\frac{\partial c_i}{\partial t} + c_i \tag{A.1}$$

and carry this into Eq. (1), obtaining

$$\frac{\partial}{\partial t}\left(\frac{1}{k}\frac{\partial c_i}{\partial t} + c_i\right) - D_{s,e}\frac{\partial}{\partial z}\left(\frac{\partial}{\partial z}\left(\frac{1}{k}\frac{\partial c_i}{\partial t} + c_i\right)\right) - \frac{1-\varepsilon}{\varepsilon}k\left(c_i - \left(\frac{1}{k}\frac{\partial c_i}{\partial t} + c_i\right)\right) = 0 \tag{A.2}$$

and after rearrangement, multiplication by k and on introducing $\delta = (1-\varepsilon)/\varepsilon$

$$\frac{\partial^2 c_i}{\partial t^2} + (\delta+1)k\frac{\partial c_i}{\partial t} - D_{s,e}\frac{\partial^3 c_i}{\partial t \partial z^2} - D_{s,e}k\frac{\partial^2 c_i}{\partial z^2} = 0. \tag{A.3}$$

To resolve the inhomogeneous boundary condition (Eq. (18)), we introduce a new function $\psi(z,t)$ as

$$\psi = c_i - c_{i0}e^{-kt} \tag{A.4}$$

with boundary conditions

$$\frac{\partial \psi}{\partial z}\Big|_{z=0} = \left(\frac{\partial}{\partial z}\left(c_i - c_{i0}e^{-kt}\right)\right)\Big|_{z=0} = \frac{\partial c_i}{\partial z}\Big|_{z=0} = 0 \tag{A.5}$$

$$\psi|_{z=l/2} = c_i|_{z=l/2} - c_{i0}e^{-kt} = c_{i0}e^{-kt} - c_{i0}e^{-kt} = 0 \tag{A.6}$$

and initial condition

$$\psi_0 = \psi_0(z,0) = \left(c_{i0} - c_{i0}e^{-kt}\right)\Big|_{t=0} = c_{i0}(z,0) - c_{i0} = 0. \tag{A.7}$$

Inserting A.4 and its temporal derivatives into A.3 following rearrangement, yields

$$\frac{\partial^2 \psi}{\partial t^2} - D_{s,e}\frac{\partial^3 \psi}{\partial t \partial z^2} - D_{s,e}k\frac{\partial^2 \psi}{\partial z^2} + (\delta+1)k\frac{\partial \psi}{\partial t} = \delta c_{i0}k^2 e^{-kt}. \tag{A.8}$$

We proceed with separation of variables on the homogeneous form of Eq. A.8, and assemble the complete solution as

$$\psi(z,t) = \psi_h(z,t) + \psi_p(t) \tag{A.9}$$

where the homogeneous solution $\psi_h(z,t)$ is a solution of

$$\frac{\partial^2 \psi}{\partial t^2} - D_{s,e}\frac{\partial^3 \psi}{\partial t \partial z^2} - D_{s,e}k\frac{\partial^2 \psi}{\partial z^2} + (\delta+1)k\frac{\partial \psi}{\partial t} = 0. \tag{A.10}$$

According to the method of separation of variables, we represent the solution of a PDE as a product of two constituents, one a function of z and the other of t

$$\psi(z,t) = Z(z) \cdot T(t). \tag{A.11}$$

We insert Eq. A.11 into Eq. A.10 and after rearrangement, separating the two functions and their derivatives, we obtain

$$\frac{Z''}{Z} = \frac{T'' + (\delta+1)kT'}{D_{s,e}T' + D_{s,e}kT}. \tag{A.12}$$

Eq. A.12 can only hold if both sides are equal to a constant. For the sake of subsequent algebra we set the constant to $-\lambda^2$. For z, we obtain

$$\frac{Z''}{Z} = -\lambda^2 \tag{A.13}$$

of which the solution is a linear combination of trigonometric functions

$$Z(z) = \sum_{m=1}^{\infty} A_m \sin(\lambda_m z) + B_m \cos(\lambda_m z) \tag{A.14}$$

while the right-hand side of A.12 can be written as

$$T'' + \left((\delta+1)k + \lambda^2 D_{s,e}\right)T' + \lambda^2 D_{s,e}kT = 0 \tag{A.15}$$

of which the characteristic polynomial is

$$\gamma_{1,2} = \frac{-\left((\delta+1)k + \lambda^2 D_{s,e}\right) \pm \sqrt{\left((\delta+1)k + \lambda^2 D_{s,e}\right)^2 - 4\lambda^2 kD_{s,e}}}{2} \tag{A.16}$$

finally giving the solution

$$T(t) = K_1 e^{\gamma_1 t} + K_2 e^{\gamma_2 t}. \tag{A.17}$$

The complete solution is thus

$$\begin{aligned}\psi_h(z,t) &= Z(z) \cdot T(t) \\ &= \sum_{m=1}^{\infty}(A_m \sin(\lambda_m z) + B_m \cos(\lambda_m z))\left(K_1 e^{\gamma_1 t} + K_2 e^{\gamma_2 t}\right).\end{aligned} \tag{A.18}$$

Note that since γ_1 and γ_2 are functions of λ_m, they get updated as well with every increment in the summation index m.

We now look for the particular solution of the inhomogeneous PDE, Eq. A.8, via the method of undetermined coefficients, of which the details we will omit. The particular solution is

$$\psi_p(t) = -c_{i0}e^{-kt}. \tag{A.19}$$

We can now complete Eq. A.9 to obtain $\psi(z,t)$

$$\psi(z,t) = \sum_{m=1}^{\infty}(A_m \sin(\lambda_m z) + B_m \cos(\lambda_m z))\left(K_1 e^{\gamma_1 t} + K_2 e^{\gamma_2 t} - c_{i0}e^{-kt}\right). \tag{A.20}$$

Next, we turn to the boundary conditions to determine coefficients A_m, B_m and eigenvalues λ_m. The following must be met

$$(A_m \sin(\lambda_m z) + B_m \cos(\lambda_m z))|_{z=l/2} = 0 \tag{A.21}$$

$$(A_m \lambda_m \cos(\lambda_m z) - B_m \lambda_m \sin(\lambda_m z))|_{z=0} = 0 \tag{A.22}$$

from Eq. A.21 follows that A_m equals 0, while from Eq. A.22 we get λ_m

$$\lambda_n = \frac{(2n+1)\pi}{l} \tag{A.23}$$

where summation index m was replaced with n, the latter running from 0 to infinity. The coefficient B_n can be calculated via the general formula for Fourier series coefficients

$$B_n = \frac{2}{l/2}\int_0^{l/2} \cos\left(\frac{(2n+1)\pi}{l}z\right)dz = \frac{4}{\pi}\frac{(-1)^n}{2n+1}. \tag{A.24}$$

Inserting B_n into Eq. A.20 and setting A_n to 0, we obtain

$$\psi(z,t) = \frac{4}{\pi} \sum_{n=0}^{\infty} \frac{(-1)^n}{2n+1} \left(K_1 e^{\gamma_1 t} + K_2 e^{\gamma_2 t} - c_{i0} e^{-kt} \right) \cos\left(\frac{(2n+1)\pi}{l} z \right). \tag{A.25}$$

For K_1 and K_2, we need two algebraic equations. One is immediately evident from Eq. A.7

$$\psi(z,0) = \frac{4}{\pi} \sum_{n=0}^{\infty} \frac{(-1)^n}{2n+1} \left(K_1 e^{\gamma_1 0} + K_2 e^{\gamma_2 0} - c_{i0} e^{-k0} \right) \cos\left(\frac{(2n+1)\pi}{l} z \right) = 0 \tag{A.26}$$

resulting in

$$K_1 + K_2 = c_{i0} \tag{A.27}$$

while the other equation introduces the extracellular concentration initial condition into the solution for the intracellular concentration. We recall Eq. A.1, and write it by replacing c_i with the correct expression following from Eq. A.4, giving

$$c_e = \frac{1}{k} \frac{\partial}{\partial t} \left(\psi + c_{i0} e^{-kt} \right) + \left(\psi + c_{i0} e^{-kt} \right) = \frac{1}{k} \frac{\partial \psi}{\partial t} + \psi. \tag{A.28}$$

Carrying out the differentiation and writing Eq. A.28 for $t = 0$ gives the second equation for K_1 and K_2

$$K_1 \left(\frac{\gamma_1}{k} + 1 \right) + K_2 \left(\frac{\gamma_2}{k} + 1 \right) = c_{e0}. \tag{A.29}$$

Solving the system of Eqs. A.27 and A.29 determines K_1 and K_2 as

$$K_1 = c_{i0} \frac{\left(\frac{c_{i0}}{c_{e0}} - 1 \right) k - \gamma_2}{\gamma_1 - \gamma_2} \tag{A.30}$$

$$K_2 = c_{i0} \frac{\left(1 - \frac{c_{i0}}{c_{e0}} \right) k + \gamma_1}{\gamma_1 - \gamma_2}. \tag{A.31}$$

Taking the constant c_{i0} out of the summation and inserting the solution for ψ into Eq. A.4, we finally obtain the expression for intracellular intrinsic solute concentration $c_i(z,t)$, already given in the main body of this paper (see Eqs. (19)–(23)).

In order to obtain the extracellular intrinsic solute concentration, we must perform a time derivative on Eq. (20), multiply it by $1/k$ and add the product to Eq. (20) (in accordance with Eq. A.1). These operations yield

$$c_e(z,t) = \frac{4c_{i0}}{\pi} \frac{1}{k} \left[\sum_{n=0}^{\infty} \frac{(-1)^n}{2n+1} \cos(\lambda_n z) \left(C_{n,1} \gamma_{n,1} e^{\gamma_{n,1} t} + C_{n,2} \gamma_{n,2} e^{\gamma_{n,2} t} + ke^{-kt} \right) - c_{i0} ke^{-kt} \right] + \\ + \frac{4c_{i0}}{\pi} \sum_{n=0}^{\infty} \frac{(-1)^n}{2n+1} \cos(\lambda_n z) \left(C_{n,1} e^{\gamma_{n,1} t} + C_{n,2} e^{\gamma_{n,2} t} - e^{-kt} \right) + c_{i0} e^{-kt}. \tag{A.32}$$

We see that the exponentials $c_{i0}\exp(-kt)$ subtract to 0. Joining the summative members with same constants together into one infinite series after dividing the first series by k, we finally obtain for extracellular intrinsic solute concentration the equation already given as Eq. (19) in the main body of this paper.

References

[1] T. Kotnik, P. Kramar, G. Pucihar, D. Miklavcic, M. Tarek, Cell membrane electroporation—part 1: the phenomenon, IEEE Electr. Insul. Mag. 28 (2012) 14–23.

[2] W. Krassowska, P.D. Filev, Modeling electroporation in a single cell, Biophys. J. 92 (2007) 404–417.

[3] W.K. Neu, J.C. Neu, Theory of electroporation, in: I.R. Efimov, M.W. Kroll, P.J. Tchou (Eds.), Cardiac Bioelectric Therapy: Mechanisms and Practical Implications, Springer, 2009.

[4] D. Miklavcic, Network for development of electroporation-based technologies and treatments: COST TD1104, J. Membr. Biol. 245 (2012) 591–598.

[5] S. Haberl, D. Miklavcic, G. Sersa, W. Frey, B. Rubinsky, Cell membrane electroporation—part 2: the applications, IEEE Electr. Insul. Mag. 29 (2013) 29–37.

[6] J. Gehl, Electroporation: theory and methods, perspectives for drug delivery, gene therapy and research, Acta Physiol. Scand. 177 (2003) 437–447.

[7] M.P. Rols, C. Delteil, M. Golzio, P. Dumond, S. Cros, J. Teissie, In vivo electrically mediated protein and gene transfer in murine melanoma, Nat. Biotechnol. 16 (1998) 168–171.

[8] A.I. Daud, R.C. DeConti, S. Andrews, P. Urbas, A.I. Riker, V.K. Sondak, et al., Phase I trial of interleukin-12 plasmid electroporation in patients with metastatic melanoma, J. Clin. Oncol. 26 (36) (2008) 5896–5903.

[9] L.M. Mir, L.F. Glass, G. Sersa, J. Teissie, C. Domenge, D. Miklavcic, et al., Effective treatment of cutaneous and subcutaneous malignant tumours by electrochemotherapy, Br. J. Cancer 77 (1998) 2336–2342.

[10] G. Sersa, D. Miklavcic, M. Cemazar, Z. Rudolf, G. Pucihar, M. Snoj, Electrochemotherapy in treatment of tumours, Eur. J. Surg. Oncol. 34 (2008) 232–240.

[11] B. Mali, T. Jarm, M. Snoj, G. Sersa, D. Miklavcic, Antitumor effectiveness of electrochemotherapy: a systematic review and meta-analysis, Eur. J. Surg. Oncol. 39 (2013) 4–16.

[12] I. Edhemovic, E.M. Gadzijev, E. Brecelj, D. Miklavcic, B. Kos, A. Zupanic, et al., Electrochemotherapy: a new technological approach in treatment of metastases in the liver, Technol. Cancer Res. Treat. 10 (2011) 475–485.

[13] A.R. Denet, R. Vanbever, V. Preat, Skin electroporation for transdermal and topical delivery, Adv. Drug Deliv. Rev. 56 (2004) 659–674.

[14] N. Pavselj, D. Miklavcic, Numerical models of skin electropermeabilization taking into account conductivity changes and the presence of local transport regions, IEEE Trans. Plasma Sci. 36 (2008) 1650–1658.

[15] S. Becker, Transport modeling of skin electroporation and the thermal behavior of the stratum corneum, Int. J. Therm. Sci. 54 (2012) 48–61.

[16] B. Zorec, V. Préat, D. Miklavčič, N. Pavšelj, Active enhancement methods for intra- and transdermal drug delivery: a review, Slov. Med. J. 82 (2013).

[17] R.V. Davalos, L.M. Mir, B. Rubinsky, Tissue ablation with irreversible electroporation, Ann. Biomed. Eng. 33 (2005) 223–231.

[18] P.A. Garcia, J.H. Rossmeisl, R.E. Neal, T.L. Ellis, R.V. Davalos, A parametric study delineating irreversible electroporation from thermal damage based on a minimally invasive intracranial procedure, Biomed. Eng. Online 10 (2011) 34.

[19] M. Fincan, F. DeVito, P. Dejmek, Pulsed electric field treatment for solid–liquid extraction of red beetroot pigment, J. Food Eng. 64 (2004) 381–388.

[20] N. López, E. Puértolas, S. Condón, J. Raso, Ignacio Álvarez, Enhancement of the solid–liquid extraction of sucrose from sugar beet (Beta vulgaris) by pulsed electric fields, LWT Food Sci. Technol. 42 (2009) 1674–1680.

[21] K.V. Loginova, M.V. Shynkaryk, N.I. Lebovka, E. Vorobiev, Acceleration of soluble matter extraction from chicory with pulsed electric fields, J. Food Eng. 96 (2010) 374–379.

[22] K. El-Belghiti, Z. Rabhi, E. Vorobiev, Kinetic model of sugar diffusion from sugar beet tissue treated by pulsed electric field, J. Sci. Food Agric. 85 (2005) 213–218.

[23] E. Puertolas, P. Hernandez-Orte, G. Sladana, I. Alvarez, J. Raso, Improvement of winemaking process using pulsed electric fields at pilot-plant scale. Evolution of chromatic parameters and phenolic content of Cabernet Sauvignon red wines, Food Res. Int. 43 (2010) 761–766.

[24] K. Loginova, M. Loginov, E. Vorobiev, N.I. Lebovka, Better lime purification of sugar beet juice obtained by low temperature aqueous extraction assisted by pulsed electric field, LWT-Food Sci. Technol. 46 (2012) 371–374.

[25] S. Toepfl, V. Heinz, D. Knorr, High intensity pulsed electric fields applied for food preservation, Chem. Eng. Process. 46 (2007) 537–546.

[26] P.Y. Phoon, F.G. Galindo, A. Vicente, P. Deimek, Pulsed electric field in combination with vacuum impregnation with trehalose improves the freezing tolerance of spinach leaves, J. Food Eng. 88 (2008) 144–148.

[27] G. Saulis, Electroporation of cell membranes: the fundamental effects of pulsed electric fields in food processing, Food Eng. Rev. 2 (2010) 52–73.

[28] A. Rieder, T. Schwartz, K. Schoen-Hoelz, S.-M. Marten, J. Suess, C. Gusbeth, et al., Molecular monitoring of inactivation efficiencies of bacteria during pulsed electric field treatment of clinical wastewater, J. Appl. Microbiol. 105 (2008) 2035–2045.

[29] C. Gusbeth, W. Frey, H. Volkmann, T. Schwartz, H. Bluhm, Pulsed electric field treatment for bacteria reduction and its impact on hospital wastewater, Chemosphere 75 (2009) 228–233.

[30] J. Sheng, R. Vannela, B.E. Rittmann, Disruption of Synechocystis PCC 6803 for lipid extraction, Water Sci. Technol. 65 (2012) 567–573.

[31] K. Dymek, P. Dejmek, V. Panarese, A.A. Vicente, L. Wadso, C. Finnie, et al., Effect of pulsed electric field on the germination of barley seeds, LWT-Food Sci. Technol. 47 (2012) 161–166.

[32] C.J. Eing, S. Bonnet, M. Pacher, H. Puchta, W. Frey, Effects of nanosecond pulsed electric field exposure on Arabidopsis thaliana, IEEE Trans. Dielectr. Electr. Insul. 16 (2009) 1322–1328.

[33] M. Kaszuba, D. McKnight, M.T. Connah, F.K. McNeil-Watson, U. Nobbmann, Measuring sub nanometre sizes using dynamic light scattering, J. Nanopart. Res. 10 (2008) 823–829.

[34] P.W. Linder, L.R. Nassimbeni, A. Polson, A.L. Rodgers, The diffusion coefficient of sucrose in water. A physical chemistry experiment, J. Chem. Educ. 53 (1976) 330.

[35] L.M. Mir, S. Orlowski, Mechanisms of electrochemotherapy, Adv. Drug Deliv. Rev. 35 (1999) 107–118.
[36] J.-M. Escoffre, B. Nikolova, L. Mallet, J. Henri, C. Favard, M. Golzio, et al., New insights in the gene electrotransfer process: evidence for the involvement of the plasmid DNA topology, Curr. Gene Ther. 12 (2012) 417–422.
[37] M. Marty, G. Sersa, J.R. Garbay, J. Gehl, C.G. Collins, M. Snoj, et al., Electrochemotherapy — an easy, highly effective and safe treatment of cutaneous and subcutaneous metastases: results of ESOPE (European Standard Operating Procedures of Electrochemotherapy) study, EJC Suppl. 4 (2006) 3–13.
[38] E. Vorobiev, N. Lebovka, Pulsed-electric-fields-induced effects in plant tissues: fundamental aspects and perspectives of applications, in: E. Vorobiev, N. Lebovka (Eds.), Electrotechnologies for Extraction from Plant Foods and Biomaterials, Springer, 2008.
[39] A. Zupanic, S. Corovic, D. Miklavcic, M. Pavlin, Numerical optimization of gene electrotransfer into muscle tissue, Biomed. Eng. Online 9 (2010).
[40] M. Golzio, J. Teissie, M.P. Rols, Direct visualization at the single-cell level of electrically mediated gene delivery, Proc. Natl. Acad. Sci. U. S. A. 99 (2002) 1292–1297.
[41] C.S. Djuzenova, U. Zimmermann, H. Frank, V.L. Sukhorukov, E. Richter, G. Fuhr, Effect of medium conductivity and composition on the uptake of propidium iodide into electropermeabilized myeloma cells, Biochim. Biophys. Acta, Biomembr 1284 (1996) 143–152.
[42] B. Gabriel, J. Teissie, Time courses of mammalian cell electropermeabilization observed by millisecond imaging of membrane property changes during the pulse, Biophys. J. 76 (1999) 2158–2165.
[43] K.C. Smith, J.C. Weaver, Electrodiffusion of molecules in aqueous media: a robust, discretized description for electroporation and other transport phenomena, IEEE Trans. Biomed. Eng. 59 (2012) 1514–1522.
[44] K.C. Smith, J.C. Weaver, Transmembrane molecular transport during versus after extremely large, nanosecond electric pulses, Biochem. Biophys. Res. Commun. 412 (2011) 8–12.
[45] J. Li, H. Lin, Numerical simulation of molecular uptake via electroporation, Bioelectrochemistry 82 (2011) 10–21.
[46] Y. Granot, B. Rubinsky, Mass transfer model for drug delivery in tissue cells with reversible electroporation, Int. J. Heat Mass Transf. 51 (2008) 5610–5616.
[47] S. Movahed, D. Li, Electrokinetic transport through the nanopores in cell membrane during electroporation, J. Colloid Interface Sci. 369 (2012) 442–452.
[48] D. Miklavcic, L. Towhidi, Numerical study of the electroporation pulse shape effect on molecular uptake of biological cells, Radiol. Oncol. 44 (2010) 34–41.
[49] M. Puc, T. Kotnik, L.M. Mir, D. Miklavcic, Quantitative model of small molecules uptake after in vitro cell electropermeabilization, Bioelectrochemistry 60 (2003) 1–10.
[50] G. Pucihar, T. Kotnik, D. Miklavcic, J. Teissie, Kinetics of transmembrane transport of small molecules into electropermeabilized cells, Biophys. J. 95 (2008) 2837–2848.
[51] M.M. Sadik, J. Li, J.W. Shan, D.I. Shreiber, H. Lin, Quantification of propidium iodide delivery using millisecond electric pulses: experiments, Biochim. Biophys. Acta 1828 (2013).
[52] J. Li, W. Tan, M. Yu, H. Lin, The effect of extracellular conductivity on electroporation-mediated molecular delivery, Biochim. Biophys. Acta 1828 (2013).
[53] N.E. Olesen, J.P. Hofgaard, N.-H. Holstein-Rathlou, M.S. Nielsen, J.C.B. Jacobsen, Estimation of the effective intercellular diffusion coefficient in cell monolayers coupled by gap junctions, Eur. J. Pharm. Sci. 46 (2012) 222–232.
[54] J. Ben Ammar, J.-L. Lanoiselle, N.I. Lebovka, E. Van Hecke, E. Vorobiev, Impact of a pulsed electric field on damage of plant tissues: effects of cell size and tissue electrical conductivity, J. Food Sci. 76 (2011) E90–E97.
[55] G. Pucihar, D. Miklavcic, T. Kotnik, A time-dependent numerical model of transmembrane voltage inducement and electroporation of irregularly shaped cells, IEEE Trans. Biomed. Eng. 56 (2009) 1491–1501.
[56] G. Pucihar, D. Miklavcic, The influence of intracellular connections on the electric field induced membrane voltage and electroporation of cells in clusters, in: O. Dossel, W.C. Schlegel (Eds.), World Congress on Medical Physics and Biomedical Engineering, vol. 25 Pt 13, Springer, New York, 2009, pp. 74–77.
[57] G. Pucihar, T. Kotnik, J. Teissie, D. Miklavcic, Electropermeabilization of dense cell suspensions, Eur. Biophys. J. Biophys. Lett. 36 (2007) 173–185.
[58] G. Pucihar, J. Krmelj, M. Reberšek, T. Napotnik, D. Miklavčič, Equivalent pulse parameters for electroporation, IEEE Trans. Biomed. Eng. 58 (2011) 3279–3288.
[59] G. Saulis, R. Saule, Size of the pores created by an electric pulse: microsecond vs millisecond pulses, Biochim. Biophys. Acta, Biomembr. 1818 (2012) 3032–3039.
[60] D. Miklavcic, K. Beravs, D. Semrov, M. Cemazar, F. Demsar, G. Sersa, The importance of electric field distribution for effective in vivo electroporation of tissues, Biophys. J. 74 (1998) 2152–2158.
[61] S. Corovic, L.M. Mir, D. Miklavcic, In vivo muscle electroporation threshold determination: realistic numerical models and in vivo experiments, J. Membr. Biol. 245 (2012) 509–520.
[62] R. Bharadwaj, J.G. Santiago, Dynamics of field-amplified sample stacking, J. Fluid Mech. 543 (2005) 57–92.
[63] M. Pavlin, G. Pucihar, M. Kanduser, The role of electrically stimulated endocytosis in gene electrotransfer, Bioelectrochemistry 83 (2012) 38–45.
[64] G. Pucihar, L.M. Mir, D. Miklavcic, The effect of pulse repetition frequency on the uptake into electropermeabilized cells in vitro with possible applications in electrochemotherapy, Bioelectrochemistry 57 (2002) 167–172.
[65] M. Pavlin, D. Miklavcic, Theoretical and experimental analysis of conductivity, ion diffusion and molecular transport during cell electroporation — relation between short-lived and long-lived pores, Bioelectrochemistry 74 (2008) 38–46.
[66] G.I. Barenblatt, V.M. Entov, V.M. Ryzhik, Theory of fluid flows through natural rocks, n.d.
[67] F. de Monte, G. Pontrelli, S. Becker, Chapter 3 — drug release in biological tissues, in: S.M. Becker, A.V. Kuznetsov (Eds.), Transport in Biological Media, Elsevier, Boston, 2013, pp. 59–118.
[68] H.S. Carslaw, J.J.C. Jaeger, Conduction of Heat in Solids, 2nd edition Oxford University Press, London, UK, 1959. (second).
[69] J. Crank, The Mathematics of Diffusion, Oxford University Press, 1979.
[70] E. Neumann, S. Kakorin, Physical chemistry theory of membrane electroporation and electrotransfer of biogenic agents, Advanced Electroporation Techniques in Biology and Medicine, 2010.
[71] F.R. Harker, R.J. Redgwell, I.C. Hallett, S.H. Murray, G. Carter, Texture of Fresh fruit, in: J. Janick (Ed.), Horticultural Reviews, John Wiley & Sons, Inc., 2010, pp. 121–224.
[72] J.W. Henshaw, Characterization and Enhancement of Interstitial Gene Transport During Electric Field-mediated Gene Delivery to Solid Tumor, ProQuest, 2007.
[73] W.M. Deen, Hindered transport of large molecules in liquid-filled pores, AIChE J 33 (1987) 1409–1425.
[74] P. Dechadilok, W.M. Deen, Hindrance factors for diffusion and convection in pores, Ind. Eng. Chem. Res. 45 (2006) 6953–6959.
[75] J. Liesche, A. Schulz, Modeling the parameters for plasmodesmal sugar filtering in active symplasmic phloem loaders, Front Plant Sci. 4 (2013).
[76] J.J.L. Higdon, G.P. Muldowney, Resistance functions for spherical particles, droplets and bubbles in cylindrical tubes, J. Fluid Mech. 298 (1995) 193–210.
[77] K. Sharma, Transport Phenomena in Biomedical Engineering: Artifical organ Design and Development, and Tissue Engineering, McGraw Hill Professional, 2010.
[78] R.O. Wayne, Plant Cell Biology: From Astronomy to Zoology, Academic Press, 2009.
[79] R.P. Joshi, Q. Hu, Evolution dynamics of pore sizes, cell volume, ionic concentrations following high-voltage pulsing, IEEE Trans. Plasma Sci. 40 (2012) 2355–2359.
[80] D.A. Stewart, I.R. Gowrishankar, J.C. Weaver, Transport lattice approach to describing cell electroporation: use of a local asymptotic model, IEEE Trans. Plasma Sci. 32 (2004) 1696–1708.
[81] C. Buttersack, W. Basler, Hydraulic conductivity of cell-walls in sugar-beet tissue, Plant Sci. 76 (1991) 229–237.
[82] L.M. Mir, Bases and rationale of the electrochemotherapy, EJC Suppl. 4 (2006) 38–44.
[83] J. Pusenjak, D. Miklavcic, Modeling of interstitial fluid pressure in solid tumor, Simul. Pract. Theory 8 (2000) 17–24.
[84] LJ. Liu, S.L. Brown, J.R. Ewing, M. Schlesinger, Phenomenological model of interstitial fluid pressure in a solid tumor, Phys. Rev. E. 84 (2011) 021919.
[85] E. Bellard, B. Markelc, S. Pelofy, F. Le Guerroue, G. Sersa, J. Teissie, et al., Intravital microscopy at the single vessel level brings new insights of vascular modification mechanisms induced by electropermeabilization, J. Control. Release 163 (2012) 396–403.
[86] T. Jarm, M. Cemazar, D. Miklavcic, G. Sersa, Antivascular effects of electrochemotherapy: implications in treatment of bleeding metastases, Expert. Rev. Anticancer. Ther. 10 (2010) 729–746.
[87] M. Golzio, J. Teissie, Direct assay of electropermeabilization in a 2D pseudo tissue, Phys. Chem. Chem. Phys. 12 (2010) 14670–14672.
[88] S. Corovic, I. Lackovic, P. Sustaric, T. Sustar, T. Rodic, D. Miklavcic, Modeling of electric field distribution in tissues during electroporation, Biomed. Eng. Online 12 (2013) 16.
[89] D. Pavliha, B. Kos, M. Marcan, A. Zupanic, G. Sersa, D. Miklavcic, Planning of electroporation-based treatments using web-based treatment-planning software, J. Membr. Biol. 246 (2013) 833–842.
[90] D. Miklavcic, S. Corovic, G. Pucihar, N. Pavselj, Importance of tumour coverage by sufficiently high local electric field for effective electrochemotherapy, EJC Suppl. 4 (2006) 45–51.
[91] B. Zorec, S. Becker, M. Rebersek, D. Miklavcic, N. Pavselj, Skin electroporation for transdermal drug delivery: the influence of the order of different square wave electric pulses, Int. J. Pharm. 457 (2013) 214–223.
[92] T. Blagus, B. Markelc, M. Cemazar, T. Kosjek, V. Preat, D. Miklavcic, et al., In vivo real-time monitoring system of electroporation mediated control of transdermal and topical drug delivery, J. Control. Release 172 (2013) 862–871.
[93] P. Chiarella, V.M. Fazio, E. Signori, Electroporation in DNA vaccination protocols against cancer, Curr. Drug Metab. 14 (2013) 291–299.
[94] M. Pavlin, V. Leben, D. Miklavcic, Electroporation in dense cell suspension — theoretical and experimental analysis of ion diffusion and cell permeabilization, Biochim. Biophys. Acta, Gen. Subj. 1770 (2007) 12–23.
[95] M. Pavlin, M. Kanduser, M. Rebersek, G. Pucihar, F.X. Hart, R. Magjarevic, et al., Effect of cell electroporation on the conductivity of a cell suspension, Biophys. J. 88 (2005) 4378–4390.
[96] M. Fincan, P. Dejmek, Effect of osmotic pretreatment and pulsed electric field on the viscoelastic properties of potato tissue, J. Food Eng. 59 (2003) 169–175.
[97] N.I. Lebovka, M.V. Shynkaryk, E. Vorobiev, Drying of potato tissue pretreated by ohmic heating, Dry. Technol. 24 (2006) 601–608.
[98] J. Kestin, M. Sokolov, W.A. Wakeham, Viscosity of liquid water in the range −8 °C to 150 °C, J. Phys. Chem. Ref. Data 7 (1978) 941–948